Dolosigranulum pigrum cooperation and competition in human nasal microbiota

Silvio D. Brugger[1, 2, 3, 8*], Sara M. Eslami[2,8], Melinda M. Pettigrew[4,8], Isabel F. Escapa[2,3], Matthew M. Henke[5], Yong Kong[6] and Katherine P. Lemon[2,7,9*]

[1]Department of Infectious Diseases and Hospital Epidemiology, University Hospital Zurich, University of Zurich, Zurich, Switzerland, CH-8006

[2]The Forsyth Institute (Microbiology), Cambridge, MA, USA, 02142

[3]Department of Oral Medicine, Infection and Immunity, Harvard School of Dental Medicine, Boston, MA, USA, 02115

[4]Department of Epidemiology of Microbial Diseases, Yale School of Public Health, New Haven, CT, USA, 06510

[5] Department of Biological Chemistry and Molecular Pharmacology, Harvard Medical School, Boston, MA, USA, 02115

[6]Department of Molecular Biophysics and Biochemistry and W.M. Keck Foundation Biotechnology Resource Laboratory, Yale University, New Haven, CT, USA, 06519

[7]Division of Infectious Diseases, Boston Children's Hospital, Harvard Medical School, Boston, MA, USA, 02115

[8]These authors contributed equally

[9]Lead Contact

*Correspondence: silvio.brugger@usz.ch and klemon@forsyth.org

Keywords: *Dolosigranulum pigrum*, *Corynebacterium*, *Staphylococcus aureus*, *Streptococcus pneumoniae*, microbe-microbe interactions, interspecies interactions, upper respiratory tract, nasal, microbiota, comparative genomics

Summary

Multiple epidemiological studies identify *Dolosigranulum pigrum* as a candidate beneficial bacterium based on its positive association with health, including negative associations with nasal/nasopharyngeal colonization by the pathogenic species *Staphylococcus aureus* and *Streptococcus pneumoniae*. To gain insight into *D. pigrum*'s functions, we used a multipronged strategy. We identified *in vivo* community-level and *in vitro* phenotypic cooperation by specific nasal *Corynebacterium* species. *D. pigrum* inhibited *S. aureus* growth *in vitro*. Whereas, *D. pigrum* plus a nasal *Corynebacterium* were needed to inhibit *S. pneumoniae* growth. Moreover, *D. pigrum* L-lactic-acid production was insufficient for this inhibition. Genomic analysis of 11 strains revealed that *D. pigrum* has a small genome (average 1.86 Mb) and multiple predicted auxotrophies, which indicate that *D. pigrum* relies on its human host and cocolonizing bacteria for key nutrients. This shift to genomic and phenotypic experimentation marks a significant advance in understanding *D. pigrum*'s role in human nasal microbiota.

Introduction

Colonization of the human nasal passages by *Staphylococcus aureus* or *Streptococcus pneumoniae* is a risk factor for infection by the colonizing bacterium at a distant body site (Bogaert et al., 2004; Kluytmans et al., 1997; von Eiff et al., 2001; Wertheim et al., 2004; Young et al., 2017). Interventions that reduce the prevalence of colonization also reduce the risk of infection and transmission, e.g., (Bode et al., 2010; Lexau et al., 2005). *S. aureus* and *S. pneumoniae* are major human pathogens that cause significant morbidity and mortality worldwide (Collaborators, 2018; Tong et al., 2015; Turner et al., 2019; Wahl et al., 2018). There are also concerns regarding rising rates of antimicrobial resistance (WHO, 2012) and the potential for long-term effects of antibiotics early in life (Schulfer and Blaser, 2015). Thus, efforts have recently focused on the identification of candidate bacteria that confer colonization resistance against *S. aureus* (Brugger et al., 2016; Janek et al., 2016; Nakatsuji et al., 2017; O'Sullivan et al., 2019; Paharik et al., 2017; Piewngam et al., 2018; Williams et al., 2019; Zipperer et al., 2016) and *S. pneumoniae* (Cardenas et al., 2019; Coleman and Cervin, 2019; Manning et al., 2016; Tano et al., 2002), with particular urgency for *S. aureus* in the absence of an effective vaccine.

Little is known about the biology of the Gram-positive, catalase-negative bacterium *Dolosigranulum pigrum,* which was first described in 1993 (Aguirre et al., 1993). However, multiple studies of the human upper respiratory tract microbiota have identified *D. pigrum* (Firmicute), colonizing with or without *Corynebacterium* species (Actinobacteria), as potentially beneficial and/or protective against colonization by *S. aureus* and *S. pneumoniae* (Biesbroek et al., 2014a; Biesbroek et al., 2014b; Bomar et al., 2016; Bosch et al., 2017; Bosch et al., 2016; Camelo-Castillo et al., 2019; Copeland et al., 2018; Escapa et al., 2018; Gan et al., 2019; Hasegawa et al., 2017; Kelly et al., 2017; Langevin et al., 2017; Lappan et al., 2018; Laufer et al., 2011; Liu et al., 2015; Man et al., 2019a; Man et al., 2019b; Perez-Losada et al., 2017; Pettigrew et al., 2012; Sakwinska et al., 2014; Salter et al., 2017; Toivonen et al., 2019; Wen et al., 2018; Zhang et al.,

2016) (reviewed in (Bomar et al., 2018; Brugger et al., 2016; Esposito and Principi, 2018; Krismer et al., 2017; Man et al., 2017)). Studies sampling either nostrils or nasopharynx show very similar results; therefore, for simplicity, we use nasal or nasal passages henceforth to denote the area inclusive of the nostrils through the nasopharynx. *D. pigrum* and *S. aureus* are inversely correlated in adult nasal microbiota (Escapa et al., 2018; Liu et al., 2015; Yan et al., 2013). Whereas, in pediatric nasal microbiota, *D. pigrum* and members of the genus *Corynebacterium* are overrepresented when *S. pneumoniae* is absent (Bomar et al., 2016; Lappan et al., 2018; Laufer et al., 2011). Moreover, children with *D. pigrum* colonization of the nasal passages are less likely to have acute otitis media (Lappan et al., 2018; Pettigrew et al., 2012) and it has been speculated that *D. pigrum*-dominated microbiota profiles might be more resistant to invasive pneumococcal disease (Camelo-Castillo et al., 2019). Furthermore, *D. pigrum* abundance in the nasal passages is inversely associated with wheezing and respiratory tract infections in infants (Biesbroek et al., 2014a). The intriguing inferences from these studies that *D. pigrum* plays a beneficial role in human nasal microbiota deserves further investigation.

In contrast to the above, there are very few reports of *D. pigrum* in association with human disease (Hoedemaekers et al., 2006; LaClaire and Facklam, 2000; Lecuyer et al., 2007; Sampo et al., 2013; Venkateswaran et al., 2014). Its frequent identification in human nasal microbiota (Bogaert et al., 2011; Bosch et al., 2017; Bosch et al., 2016; Camarinha-Silva et al., 2012a; Camarinha-Silva et al., 2012b; Camelo-Castillo et al., 2019; Caputo et al., 2019; Chonmaitree et al., 2017; Copeland et al., 2018; De Boeck et al., 2017; Escapa et al., 2018; Gan et al., 2019; Kelly et al., 2017; Langevin et al., 2017; Lappan et al., 2018; Laufer et al., 2011; Liu et al., 2015; Luna et al., 2018; Man et al., 2019b; Peterson et al., 2016; Sakwinska et al., 2014; Salter et al., 2017; Song et al., 2019; Teo et al., 2015; Toivonen et al., 2019; Walker et al., 2019; Wen et al., 2018; Wos-Oxley et al., 2010; Zhang et al., 2016) coupled with its rare association with infection are consistent with *D. pigrum* functioning as a commensal, and possibly as a mutualist, of humans–

87 –characteristics that support its potential for future use as a therapeutic. However, its metabolism
88 and its interplay with other nasal bacteria remain uncharted territory. Using a multipronged
89 approach, we have made significant advances in these areas. First, we identified, at the species-
90 level, candidate bacterial interactors with *D. pigrum* by analyzing nasal microbiota datasets from
91 adults and children. Second, we delineated key metabolic features of *D. pigrum*'s core genome
92 based on 11 distinct *D. pigrum* strains. Third, we used *in vitro* phenotypic assays to show that *D.*
93 *pigrum* exhibits distinct interaction phenotypes with nasal *Corynebacterium* species, *S. aureus*
94 and *S. pneumoniae*. These new insights into *D. pigrum*'s functional capacity advance the field
95 from compositional analysis to genomic and phenotypic experimentation on a potentially
96 beneficial bacterial resident of the human upper respiratory tract.

97

98 **Results**

99 **Individual species of *Corynebacterium* are positively associated with *D. pigrum* in the**
100 **nasal microbiota of both adults and children.** Multiple 16S rRNA gene-based microbiota
101 studies identify genus-level associations between *Dolosigranulum* and *Corynebacterium*, e.g.,
102 (Biesbroek et al., 2014a; Biesbroek et al., 2014b; Bosch et al., 2017; Copeland et al., 2018; de
103 Steenhuijsen Piters and Bogaert, 2016; Hasegawa et al., 2017; Lappan et al., 2018; Teo et al.,
104 2015). *D. pigrum* is the only member of its genus and data regarding species-level associations
105 with *Corynebacterium* and other taxa are lacking. Therefore, we identified bacterial species that
106 display differential relative abundance in the absence or presence of *D. pigrum* sequences. As a
107 prerequisite, we identified two nostril datasets with V1-V2/V1-V3 16S rRNA gene sequences,
108 regions that contain sufficient information for species-level identification of most nasal-associated
109 bacteria (Escapa et al., 2018; Laufer et al., 2011). After parsing sequences into species-level
110 phylotypes, we interrogated each dataset using Analysis of Composition of Microbiomes

(ANCOM) (Mandal et al., 2015). In the nostrils of 210 adult participants from the Human Microbiome Project (HMP), four *Corynebacterium* species—*C. accolens, C. propinquum, C. pseudodiphtheriticum* and an unresolved supraspecies of *C. accolens-macginleyi-tuberculostearicum*—exhibited increased differential relative abundance in the presence of *D. pigrum* (**Figure 1A, panels ii-v and Table S1**). In the nostrils of 99 children ages 6 and 78 months (Laufer et al., 2011), *Corynebacterium pseudodiphtheriticum* exhibited increased differential relative abundance in the presence of *D. pigrum*, as did *Moraxella nonliquefaciens* (**Figure 1B**). Together, these results from children and adults identify a positive relationship between *D. pigrum* and individual species of *Corynebacterium* in human nasal microbiota, with a positive association of *D. pigrum* and *C. pseudodiphtheriticum* across age groups.

Nasal *Corynebacterium* species enhance the growth of *D. pigrum in vitro*. Various types of microbe-microbe interactions could underlie the positive *in vivo* association between *D. pigrum* and individual *Corynebacterium* species in human nasal microbiota (**Figure 1**). One being a direct interaction between these species mediated by diffusible compounds. To test this possibility, we quantified *D. pigrum* growth yields on unconditioned agar medium compared to on cell-free agar medium conditioned by growth of *C. pseudodiphtheriticum, C. propinquum* or *C. accolens*. Conditioning medium with any of these three nasal *Corynebacterium* species increased the yield (measured as colony forming units, CFUs) of two *D. pigrum* strains (CDC 4709-98 and KPL1914) by one to two orders of magnitude compared to growth on unconditioned agar medium (**Figures 2A** and **2B**). Additionally, one strain of *C. pseudodiphtheriticum* (**Figure 2A**) and the *C. accolens* strain (**Figure 2B**) increased the growth yield of *D. pigrum* CDC 2949-98, a strain with a higher baseline growth yield. Results of this phenotypic interaction assay are consistent with unilateral cooperation of nasal *Corynebacterium* species—*C. pseudodiphtheriticum, C. propinquum* or *C. accolens*—with *D. pigrum* in the nostril microbiota of both children and adults and support the observed positive *in vivo* community-level relationships.

Although positive interactions between *C. accolens* and *D. pigrum* prevailed *in vivo* in adults (**Figure 1A, panel ii**)*, in vitro* we observed both positive and negative interactions between *D. pigrum* and *C. accolens* depending on the assay conditions. For example, we observed increased *D. pigrum* growth yield on a semi-permeable membrane on *C. accolens* cell-free conditioned agar medium (CFCAM) of Brain Heart Infusion (BHI) supplemented with triolein (**Figure 2B**). In contrast, *D. pigrum* was inhibited when inoculated directly onto *C. accolens* CFCAM (**Table S2**). Like *S. pneumoniae, D. pigrum* belongs to the order Lactobacillales; the inhibition was reminiscent of our previous research demonstrating that *C. accolens*' triacylglycerol lipase, LipS1, releases free fatty acids from model host epithelial-surface triacylglycerols, such as triolein, to inhibit *S. pneumoniae in vitro* (Bomar et al., 2016). We observed that oleic acid also inhibited *D. pigrum* (**Table S3**). Thus, *in vitro* data show *C. accolens* can both inhibit the growth of *D. pigrum* by releasing antibacterial free fatty acids such as oleic acid from host triacylglycerols (**Tables S2 and S3**) and enhance the growth of *D. pigrum* by releasing as-yet unidentified factor(s) (**Figure 2B**). These results point to the existence of a complex set of the molecular interactions between these two species.

***D. pigrum* inhibits *S. aureus* growth.** Researchers have sought to identify commensal bacteria that provide colonization resistance to pathobionts such as *S. aureus* (Janek et al., 2016; Nakatsuji et al., 2017; O'Sullivan et al., 2019; Paharik et al., 2017; Piewngam et al., 2018; Williams et al., 2019; Zipperer et al., 2016) (reviewed in (Brugger et al., 2016)). In contrast to the positive association between *D. pigrum* and specific *Corynebacterium* species, ANCOM analysis of adult nostril microbiota datasets revealed decreased differential relative abundance of *S. aureus* in the presence of *D. pigrum* (**Figure 1A**). Direct antagonism could explain this observation. Therefore, we assayed for the effect of *D. pigrum* on *S. aureus* and observed inhibition of *S. aureus* when it was inoculated adjacent to a pregrown inoculum of *D. pigrum* on agar medium (**Figure 3**). (We gave *D. pigrum* a head-start to compensate for its slower growth rate *in vitro.*) To assess whether

this *D. pigrum* inhibition of *S. aureus* was strain specific, we tested nine additional *D. pigrum* strains. All nine also inhibited *S. aureus* (**Figure S1**). This, plus the observed cooperation from nasal *Corynebacterium* species for *D. pigrum* growth yield (**Figure 2**), led us to explore the genetic capacity of *D. pigrum.*

The genomes of 11 *D. pigrum* strains reveal a small genome and high degree of sequence conservation consistent with a highly host-adapted bacterium. We analyzed one publicly available genome of *D. pigrum* (ATCC51524) and sequenced 10 additional strains. The 10 sequenced strains were selected to ensure representation of distinct strains (see Methods). The 11 *D. pigrum* strain genomes had an average size of 1.86 Mb (median 1.88 Mb) with 1693 predicted coding sequences and a mean GC content of 39.6% (**Tables 1** and **S4**). This genome size is consistent with *D. pigrum* being a highly host-adapted bacterium with reduced biosynthetic capacities (Pfeiler and Klaenhammer, 2007) and is similar to or slightly smaller than other Firmicutes commonly found in human oral, respiratory and skin environments, e.g., (Galac et al., 2017; Hilty et al., 2014; Suzuki et al., 2012; Tettelin et al., 2001).

From the nucleotide sequences of these 11 strains, an estimate of the upper bound of a conservative core genome for *D. pigrum* is 1200 coding sequencing (CDS) based on the overlap of three ortholog prediction algorithms (**Figure S2**). Two of these algorithms together estimated a lower bound of 1513 CDS for the *D. pigrum* accessory genome within a pangenome of 2729 CDS (based on an estimated core of 1216 CDS) (**Figure S3** and **Table S5**). Similarity matrices of the core genes and proteins from the 11 *D. pigrum* strains revealed a high degree of nucleotide (≥97%) and amino acid (≥96.8%) sequence conservation (**Figure S4A** and **S4B**, respectively).

To gain insight into the chromosomal structure of *D. pigrum*, we closed the genomes of two strains, CDC 4709-98 (**Figure S5A**) and KPL1914 (**Figure S5B**) using SMRT sequencing. MAUVE alignment revealed large blocks of synteny between these two closed genomes (**Figure**

185 **4**). Synteny analysis of the bidirectional best-hits core proteins from the RAST annotation revealed
186 1143 syntenic clusters (of 1206 total BDBH clusters). Ring plots using the closed genome of CDC
187 4709-98 as the reference (**Figure S5A**), because it is 5% (97 kb) larger than that of KPL1914,
188 showed discrete areas of sequence absence in KPL1914 (**Figure S5C**) along with large areas of
189 conservation. Similar areas of absence were visible when the other 9 strains were also compared
190 to CDC 4709-98 (**Figure S5D**).

191 **A core-genome phylogeny reveals relationships between the 11 *D. pigrum* strains.** In 16S
192 rRNA gene-based phylogenies, *D. pigrum* clades with other lactic acid bacteria and shares the
193 closest node with *Alloiococcus otitis* (aka *A. otitidis*); both species are within the family
194 *Carnobacteriaceae* (order *Lactobacillales*) (Yarza et al., 2008). Genomic content also identified
195 *Alloiococcus* as its closest genome-sequenced neighbor by RAST. Using *A. otitis* ATCC 51267
196 as an outgroup, a core-genome, maximum likelihood-based phylogeny revealed a monophyletic
197 *D. pigrum* clade (**Figure S6**). Although the 11 strains were isolated from different individuals in
198 different geographic regions, mostly in the late 1990s (**Table 1**), there was a relatively small
199 evolutionary distance. We next explored the metabolic capacity of *D. pigrum's* core genome to
200 gain insights into its functions in human nasal microbiota.

201 **Whole genome sequencing indicates that *D. pigrum* metabolizes carbohydrates via**
202 **homofermentation to lactic acid.** It is proposed that *D. pigrum* utilizes lactic acid production as
203 a mechanism for competition in the nasal passages (de Steenhuijsen Piters and Bogaert, 2016).
204 Lactic acid bacteria mainly perform either homo- or heterofermentation of carbohydrates (Kandler,
205 1983). Therefore, we examined the genomic capacity of *D. pigrum* for carbohydrate metabolism
206 and observed patterns of gene presence and absence that are consistent with homofermentation
207 of carbohydrates to lactic acid. *D. pigrum* genomes lacked genes required for a complete
208 tricarboxylic acid -cycle, which is consistent with fermentation. Moreover, we identified genes
209 encoding a complete glycolytic pathway in all 11 strains that are consistent with homofermentation

(supplemental text). All 11 strains harbored a predicted L-lactate-dehydrogenase (EC 1.1.1.27), which catalyzes the reduction of pyruvate to lactate regenerating NAD+ for glycolysis (GAPDH step), consistent with homofermentation to L-lactate as the main product of glycolysis. Supporting this, we detected lactate production by *D. pigrum* during *in vitro* cultivation (**Figure 5A**).

***D. pigrum* production of lactic acid is unlikely to be the primary mechanism for the negative association with *S. pneumoniae* in pediatric nasal microbiota.** *D. pigrum* lactic acid production has been proposed as a mechanism to explain epidemiologic observations of negative associations between *D. pigrum* and *S. pneumoniae* (de Steenhuijsen Piters and Bogaert, 2016). Under nutrient rich conditions *in vitro*, three tested strains of *D. pigrum* produced from 5.7 to 8.2 mM of L-lactic acid with strain KPL1914 producing the highest concentration (**Figure 5A**). Therefore, we assayed for growth of *S. pneumoniae* in *D. pigrum* KPL1914 CFCM compared to in BHI broth supplemented with varying concentrations of L-lactic acid. Three of the four *S. pneumoniae* strains tested showed some growth in 22 mM lactic acid (**Figure 5B**), and all strains displayed more growth in BHI supplemented with 11 mM L-lactic acid than in the *D. pigrum* KPL1914 CFCM, which had 7.5 mM of *D. pigrum*-produced L-lactic acid (**Figure 5B**). Thus, the restriction of *S. pneumoniae* growth in *D. pigrum* CFCM is unlikely to be due to *D. pigrum* production of lactic acid. More likely, it reflects competition for nutrients since fresh medium was not added to the CFCM, which, therefore, would have a lower concentration of sugars than BHI broth. However, *D. pigrum* production of a toxin and/or an antipneumococcal compound in BHI broth cannot be excluded. These results indicate that *D. pigrum* production of lactic acid in human nasal passages is unlikely to be the primary molecular mechanism underlying the decreased relative abundance of *S. pneumoniae* in children's nasal passages when *D. pigrum* is present.

D. pigrum is negatively associated with S. *aureus* in adult nostrils (Escapa et al., 2018; Liu et al., 2015; Yan et al., 2013) and *D. pigrum* excreted a diffusible activity that inhibited *S. aureus* growth on BHI agar (**Figures 3** and **S1**). Therefore, we also tested the *in vitro* effect of L-lactic acid on

two strains of *S. aureus*. Both grew in BHI supplemented with 22 mM L-lactic acid, with a statistically significant decrease in growth in 33 mM L-lactic acid (**Figure 5C**). Thus, under the tested conditions *D. pigrum* does not produce enough L-lactic acid to restrict *S. aureus* growth. In contrast to *S. pneumoniae*, we would not expect depletion of sugars to impact *S. aureus* growth in CFCM given its broader repertoire of energy source utilization options, e.g., amino acids, and indeed both *S. aureus* strains showed no decrease in growth in *D. pigrum* CFCM. This also points to a difference in *D. pigrum* production of the anti-*S. aureus* activity during growth on BHI agar medium (**Figure 3; Fig S1**) versus in BHI broth. Excretion of metabolites may vary during growth in liquid versus on agar medium and the mechanism of the *D. pigrum* anti-*S. aureus* activity is yet-to-be identified.

***D. pigrum* is a predicted auxotroph for some amino acids, polyamines and enzymatic cofactors.** The nasal environment is low and/or lacking in key nutrients such as methionine (Krismer et al., 2014). To gain insight into how *D. pigrum* functions in the nose, we examined all 11 genomes and found evidence of auxotrophy for some amino acids, polyamines and required enzymatic cofactors (supplemental text). For example, all 11 strains lacked complete predicted biosynthetic pathways for methionine and arginine but encoded putative degradation pathways for these, suggesting these amino acids are acquired exogenously. Additionally, all 11 genomes encoded predicted transporters for polyamines, such as putrescine and spermidine, but not the genes for a complete polyamine biosynthetic pathway. In terms of enzyme cofactors, *D. pigrum* genomes lacked genes for *de novo* synthesis of niacin/nicotinate/nicotinamide but encoded a putative transporter. Similarly, all 11 strains lacked genes for the biosynthesis of cobalamin (B12), thiamine (B1), pyridoxine (B6) and biotin (B7), with predicted biotin transport/uptake genes, and 10 of 11 lacked a riboflavin (B2) synthesis cluster (all except CDC 4199-99). Similarly, a complete set of folate biosynthesis genes are lacking in all 11, which appear to encode folate salvage pathways, along with folate to tetrahydrofolate conversion via dihydrofolate reductase (EC

1.5.1.3). Likely auxotrophy for the above points to nutrients that must be available either from the host or from neighboring microbes in human nasal passages.

***D. pigrum* encodes mechanisms for acquiring essential metal cofactors from the host environment.** The nasal environment is low on essential metal ions such as iron, zinc and manganese and host metal sequestration using lactoferrin and calprotectin is an important defense mechanism against bacterial growth. Bacteria have acquired mechanisms to escape this nutritional immunity (Krismer et al., 2014; Krismer et al., 2017). We therefore searched for genes predicted to encode for siderophores and transporters for heme, manganese and zinc. All 11 *D. pigrum* genomes harbored a predicted iron compound ABC uptake transporter ATP-binding protein (hemin uptake system subsystem) and a manganese ABC-type transporter. Additionally, six of the CDC strains (4294-98, 4420-98, 4545-98, 4199-99, 4791-99, 4792-99) had predicted ferric iron ABC transporter and/or iron compound ABC uptake transporter genes.

Our analysis of the genomes of 11 distinct strains provided key insights into the biology and environment of *D. pigrum*. It did not, however, identify a molecular mechanism for the negative association between *D. pigrum* and *S. pneumoniae*. This led us to investigate whether a cooperative interaction with nasal *Corynebacterium* species might be key to the negative association of *D. pigrum* and *S. pneumoniae*, since many pediatric nasal microbiota composition studies also detect a positive association between *D. pigrum* and *Corynebacterium*, e.g., (**Figure 1B**) and (Biesbroek et al., 2014a; Biesbroek et al., 2014b; Bosch et al., 2017; Copeland et al., 2018; de Steenhuijsen Piters and Bogaert, 2016; Hasegawa et al., 2017; Lappan et al., 2018; Teo et al., 2015).

Together *D. pigrum* and *C. pseudodiphtheriticum* inhibit *S. pneumoniae* growth. Since *C. pseudodiphtheriticum* displayed increased differential relative abundance in the presence of *D. pigrum* (**Figure 1**), we investigated the effect of a mixed *in vitro* population of *D. pigrum* and *C.*

pseudodiphtheriticum on *S. pneumoniae* growth. Agar medium conditioned with a coculture of *C. pseudodiphtheriticum* strain KPL1989 and *D. pigrum* strain CDC4709-98 inhibited *S. pneumoniae* growth, whereas agar medium conditioned with a monoculture of either species did not (**Figures 6** and **S7**). This is consistent with cocultivation resulting in either a greater level of nutrient competition than monoculture of either commensal alone or in the production of diffusible compound(s) toxic/inhibitory to *S. pneumoniae* by one or both of the commensal species when grown together. Along with the *Corynebacterium* species enhancement of *D. pigrum* growth yield (**Figure 2**) and the *D. pigrum* inhibition of *S. aureus* growth (**Figure 3**), these data indicate that the negative associations of *D. pigrum* with *S. aureus* and *S. pneumoniae* are mediated by different molecular mechanisms.

The accessory genome of 11 *D. pigrum* strains contains a diversity of biosynthetic gene clusters predicted to encode antibiotics. Data presented above indicate that lactic acid alone is unlikely to account for the negative associations of *D. pigrum* with *S. aureus* and with *S. pneumoniae* in *in vivo* community composition data. Also, *D. pigrum*'s competitive interactions with these two species may well be mediated by different mechanisms. Therefore, we delved into the functional capacity of *D. pigrum*, including the accessory genome of the 11 sequenced strains. What emerged was a diversity of biosynthetic gene clusters (BGCs) (**Table S6 and Figure S8**), including a diversity of BGCs predicted to encode candidate antibiotics. Strikingly, although 10 of 10 strains tested displayed inhibition of *S. aureus* growth *in vitro* (**Figure S1**), there was no single BGC common to all 10 strains that might encode a compound with antibiotic activity. Based on this, we hypothesize that *D. pigrum* uses a diverse repertoire of BGCs to produce bioactive molecules that play key roles in interspecies interactions with its microbial neighbors, e.g., for niche competition, and potentially with its host. This points to a new direction for future research on the functions that underlie the positive associations of *D. pigrum* in human nasal microbiota with health.

Discussion

D. pigrum is associated with health in multiple genus-level compositional studies of human URT/nasal passage microbiota. The above species-level genomic and phenotypic experimental data mark a significant advance in the study of *D. pigrum* and set the stage for future mechanistic research. Here, in nasal passage microbiota datasets, we identified positive associations of *D. pigrum* with specific species of *Corynebacterium* in adults and children and a negative association of *D. pigrum* with *S. aureus* in adults (**Figure 1**). We observed phenotypic support for these associations during *in vitro* growth via cooperation from three common nasal *Corynebacterium* species that increased *D. pigrum* growth yields (**Figure 2**) and by *D. pigrum* inhibition of *S. aureus* (**Figure 3**). Our genomic analysis revealed auxotrophies consistent with reliance on cocolonizing microbes and/or the human host for key nutrients. Genomic analysis also showed an aerotolerant anaerobe that performs homofermentation to lactate. However, *D. pigrum* lactate production (**Figure 5A**) was insufficient to inhibit either *S. aureus* (**Figure 5B**) or *S. pneumoniae* (**Figure 5C**), and is, therefore, unlikely to be the sole contributor to negative associations with *S. pneumoniae* and *S. aureus in vivo*. Consistent with the multiple reports of a negative association between *D. pigrum*, usually in conjunction with the genus *Corynebacterium*, and *S. pneumoniae*, we observed that cocultivation of *D. pigrum* and *C. pseudodiphtheriticum* produced a diffusible activity that inhibited *S. pneumoniae* (**Figures 6** and **S7**). Finally, we identified a surprisingly diverse repertoire of BGCs in 11 *D. pigrum* strains, revealing potential mechanisms for niche competition that were previously unrecognized and opening up a new line of investigation in the field. The *in vitro* interactions of *D. pigrum* with *S. aureus* and with *S. pneumoniae* support inferences from composition-level microbiota data of competition between *D. pigrum* and each pathobiont. However, these interactions differed *in vitro*. *D. pigrum* alone inhibited *S. aureus* but *D. pigrum* plus *C. pseudodiphtheriticum*, together, inhibited *S. pneumoniae*. This points to a more complex

334 set of interactions among these specific bacterial members of the human nasal microbiota, which
335 likely exists in the context of a network of both microbe-microbe and microbe-host interactions.
336 To date, mechanisms for only a few such interactions are described. For example, a *C. accolens*
337 triacylglycerol lipase (LipS1) releases antipneumococcal free fatty acids from model host surface
338 triacyclglycerols *in vitro* pointing to habitat modification as a possible contributor to S*. pneumoniae*
339 colonization resistance (Bomar et al., 2016).

340 Multiple mechanisms could result in *D. pigrum* inhibition of *S. aureus in vitro* including nutrient
341 competition, excretion of a toxic primary metabolite or of an anti-*S. aureus* secondary metabolite
342 (i.e., an antibiotic). The latter is intriguing because the diverse repertoire of BGCs among the 11
343 *D. pigrum* strains includes predicted lanthipeptides and bacteriocins. For example, 4 of the 11
344 strains harbored putative type II lanthipeptide biosynthetic gene clusters. These clusters are
345 characterized by the presence of the LanM enzyme, containing both dehydration and cyclization
346 domains needed for lanthipeptide biosynthesis (Repka et al., 2017). Alignment of these enzymes
347 with the enterococcal cytolysin LanM revealed conserved catalytic residues in both domains
348 (Dong et al., 2015). Cleavage of the leader portion of the lanthipeptide is necessary to produce
349 an active compound and the presence of peptidases and transporters within these BGCs
350 suggests these *D. pigrum* strains might secrete an active lanthipeptide, which could play a role in
351 niche competition with other microbes. Additionally, 8 of the 11 *D. pigrum* genomes examined
352 contain putative bacteriocins, or bactericidal proteins and peptides. Intriguingly, the *D. pigrum*
353 strains (CDC4709-98, CDC39-95, KPL1914) exhibiting the strongest inhibition of *S. aureus*
354 (**Figure S1**), were the only strains that contained both a lanthipeptide BGC and a bacteriocin,
355 further indicating that *D. pigrum* may employ multiple mechanisms to inhibit *S. aureus* growth.

356 Mechanisms are coming to light for how other nasal bacteria interact with *S. aureus*. For example,
357 commensal *Corynebacterium* species excrete a to-be-identified substance that inhibits *S. aureus*
358 autoinducing peptides blocking *agr* quorum sensing (QS) and shifting *S. aureus* shifts towards a

359 commensal phenotype (Ramsey et al., 2016). Also, the to-be-identified mechanism of *C.*
360 *pseudodiphtheriticum* contact-dependent inhibition of *S. aureus* is mediated through phenol
361 soluble modulins (PSM), the expression of which increases during activation of *agr* QS (Hardy et
362 al., 2019). Within broader *Staphylococcus-Corynebacterium* interactions, *C. propinquum*
363 outcompetes coagulase-negative *Staphylococcus* (CoNS), but not *S. aureus*, for iron *in vitro* using
364 the siderophore dehydroxynocardamine, the genes for which are transcribed *in vivo* in human
365 nostrils (Stubbendieck et al., 2019). Interphylum Actinobacteria-Firmicutes interactions also occur
366 between *Cutibacterium acnes* and *Staphylococcus* species (reviewed in (Brugger et al., 2016)).
367 For example, some strains of *C. acnes* produce an anti-staphylococcal thiopeptide, cutimycin, *in*
368 *vivo* and the presence of the cutimycin BGC is correlated with microbiota composition at the level
369 of the individual human hair follicle (Claesen et al., 2019). Of note, Actinobacteria competition
370 with coagulase-negative *Staphylococcus* species could also have network-mediated (indirect)
371 effects on *S. aureus* via the well-known competition among *Staphylococcus* species (reviewed in
372 (Parlet et al., 2019)), which can be mediated by antibiotic production, e.g., (Janek et al., 2016;
373 Nakatsuji et al., 2017; O'Sullivan et al., 2019; Zipperer et al., 2016), interference with *S. aureus*
374 *agr* QS (Otto et al., 2001; Otto et al., 1999; Paharik et al., 2017; Williams et al., 2019) or
375 extracellular protease activity (Iwase et al., 2010), among other means (Brugger et al., 2016).
376 Further rounding out the emerging complexity of microbe-microbe interactions in nasal microbiota,
377 multiple strains of *Staphylococcus*, particularly *S. epidermidis*, inhibit the *in vitro* growth of other
378 nasal and skin bacteria, including *D. pigrum*, via to-be-identified mechanisms (Janek et al., 2016).
379 The above points to a wealth of opportunity to use human nasal microbiota as a model system to
380 learn how bacteria use competition to shape their community.

381 Direct cooperation could contribute to the observed positive associations between bacterial
382 species in epidemiological microbiome studies. Conditioning medium with any of the three nasal
383 *Corynebacterium* species positively associated with *D. pigrum in vivo* in human nasal microbiota

384 (**Figure 1**) enhanced the growth yield of some *D. pigrum* strains (**Figure 2**). This is possibly by
385 excretion of a limiting nutrient or by removal of a toxic medium component. The genomic
386 predictions of auxotrophy (above and supplemental text) might favor nasal *Corynebacterium*
387 species providing cooperation to *D. pigrum* by excretion of a limiting nutrient. Indeed, mass
388 spectrometry indicates a number of nutrients are limiting in the nose (Krismer et al., 2014).

389 Among the limitations of this study are these four. First, we analyzed the genomes of 11 strains,
390 and these were primarily isolated in the setting of disease. It is unclear whether these strains were
391 contaminants or pathogenic contributors (LaClaire and Facklam, 2000) but, with the exception of
392 keratitis, *D. pigrum* strains are infrequently associated with disease (Haas et al., 2012; Hall et al.,
393 2001; Hoedemaekers et al., 2006; Johnsen et al., 2011; Lecuyer et al., 2007; Lin et al., 2006;
394 Sampo et al., 2013; Venkateswaran et al., 2014). These 11 *D. pigrum* strains encoded only a few
395 potential virulence factors, which is consistent with *D. pigrum* acting primarily as a mutualistic
396 species of humans. Second, the ongoing search for a fully defined chemical medium permissive
397 for *D. pigrum* growth precluded experimental verification of predicted auxotrophies and further
398 investigation of how nasal *Corynebacterium* enhance *D. pigrum* growth yields. Third, our
399 approach assessed a limited set of possible interactions from among the complex multispecies
400 interplay discussed above that includes other common bacterial members of the nasal passages.
401 Fourth, to date, there is no animal model for nasal colonization with *D. pigrum* and
402 *Corynebacterium* species, which stymies directly *in vivo* testing the hypothesis of pathobiont
403 inhibition and points to another area of need within the nasal microbiome field.

404 In summary, we validated *in vivo* associations from human bacterial microbiota studies with
405 functional assays which support the hypothesis that *D. pigrum* is a mutualist, rather than a purely
406 commensal bacterium, with respect to its human host. The next step will be to identify the
407 molecular mechanisms of those interactions and to assess their role in the human host. Such
408 work could establish the premise for future studies to investigate the therapeutic potential of *D.*

409 *pigrum* as a topical nasal probiotic for use in patients with recurrent infections with *S. pneumoniae*,
410 possibly in conjunction with a nasal *Corynebacterium* species, or *S. aureus,* in conjunction with
411 established *S. aureus* decolonization techniques (Fritz et al., 2012).

Materials and Methods.

Species-level reanalysis of a pediatric nostril microbiota dataset. Laufer et al. analyzed nostril swabs collected from 108 children ages 6 to 78 months (Laufer et al., 2011). Of these, 44% were culture positive for *S. pneumoniae* and 23% were diagnosed with otitis media. 16S rRNA gene V1-V2 sequences were generated using Roche/454 with primers 27F and 338R. We obtained 184,685 sequences from the authors, of which 94% included sequence matching primer 338R and 1% included sequence matching primer 27F. We performed demultiplexing in QIIME (Caporaso et al., 2010b) (split_libraries.py) filtering reads for those ≥250 bp in length, quality score ≥30 and with barcode type hamming_8. Then, we eliminated sequences from samples for which there was no metadata (n=108 for metadata) leaving 120,963 sequences on which we performed *de novo* chimera removal in QIIME (USEARCH 6.1) (Edgar, 2010; Edgar et al., 2011), yielding 120,274 16S rRNA V1-V2 sequences. We then aligned the 120,274 chimera-cleaned reads in QIIIME (PyNAST) (Caporaso et al., 2010a), using eHOMDv15.04 (Escapa et al., 2018) as a reference database, and trimmed the reads using “o-trim-uninformative-columns-from-alignment” and “o-smart-trim” scripts (Eren et al., 2015). 116,620 reads (97% of the chimera-cleaned) were recovered after the alignment and trimming steps. After these initial cleaning steps, we retained only the 99 samples with more than 250 reads. We analyzed this dataset of 99 samples with a total of 114,909 reads using MED (Eren et al., 2015) with minimum substantive abundance of an oligotype (-M) equal to 4 and maximum variation allowed in each node (-V) equal to 6 nt, which equals 1.6% of the 379-nucleotide length of the trimmed alignment. Of the 114,909 sequences, 82.8% (95,164) passed the -M and -V filtering and are represented in the MED output. Oligotypes were assigned taxonomy in R with the dada2::assignTaxonomy() function (an implementation of the naïve Bayesian RDP classifier algorithm with a kmer size of 8 and a bootstrap of 100) (Callahan et al., 2016; Wang et al., 2007) using the eHOMDv15.1 V1-V3 Training Set (version 1)

(Escapa et al., 2018) and a bootstrap of 70. We then collapsed oligotypes within the same species/supraspecies yielding the data shown in **Table S7**.

Microbiota community comparison (Figure 1). The pediatric 16S rRNA gene V1-V2 dataset analyzed at species level here (**Table S7**), as well as the HMP adult 16S rRNA gene V1-V3 dataset previously analyzed at species level (Table S7 in (Escapa et al., 2018)) were used as input for the ANCOM analysis, including all identified taxa (i.e., we did not remove taxa with low relative abundance). ANCOM (version 1.1.3) was performed using the presence or absence of *D. pigrum* as group definer. ANCOM default parameters were used (sig = 0.05, tau = 0.02, theta = 0.1, repeated = FALSE) except that we performed a correction for multiple comparisons (multcorr = 2), instead of using the default no correction (multcorr = 3) (Mandal et al., 2015).

Ethics statement. We isolated *D. pigrum* KPL1914 and *C. pseudodiphtheriticum* KPL1989 from the nostril of an adult as part of a protocol to study the bacterial microbiota of the nostrils of healthy adults that was initially approved by the Harvard Medical School Committee on Human Studies (Lemon et al., 2010), and subsequently approved by the Forsyth Institute Institutional Review Board.

Cultivation from frozen stocks. Bacterial strains were cultivated as described here unless stated otherwise. Across the various methods, strains were grown at 37°C with 5% CO_2 unless otherwise noted. *D. pigrum* strains were cultivated from frozen stocks on BBL Columbia Colistin-Nalidixic Acid (CNA) agar with 5% sheep blood (BD Diagnostics) for 2 days. *Corynebacterium* species were cultivated from frozen stocks on BHI agar (*C. pseudodiphtheriticum* and *C. propinquum*) or BHI agar supplemented with 1% Tween80 (*C. accolens*) for 1 day. Resuspensions described below were made by harvesting colonies from agar medium and resuspending in 1X phosphate buffered saline (PBS).

Growth yield of *D. pigrum* on a membrane atop media conditioned by growth of *Corynebacterium* species (Figure 2). Each *Corynebacterium* strain was resuspended from growth on agar medium to an optical density at 600 nm (OD_{600}) of 0.50 in 1x PBS. Then 100 μL of each resuspension was individually spread onto a 0.2-μm, 47-mm polycarbonate membrane (EMD Millipore, Billerica, MA) atop 20 mL of either BHI agar for *C. pseudodiphtheriticum* and *C. propinquum* or BHI agar supplemented with Triolein (CAS # 122-32-7, Acros) spread atop the agar medium, as previously described (Bomar et al., 2016), for *C. accolens*. After 2 days, membranes with *Corynebacterium* cells were removed, leaving cell-free conditioned agar medium (CFCAM). On each plate of CFCAM, we placed a new membrane onto which we spread 100 μL of *D. pigrum* cells that had been resuspended to an OD_{600} of 0.50 in 1x PBS. After 2 days, membranes with *D. pigrum* were removed, placed in 3 mL 1x PBS, and vortexed for 1 min. to resuspend cells. Resuspensions were diluted 1:10 six times, dilutions were inoculated onto BBL CNA agar with 5% sheep blood and colony forming units (CFUs) were enumerated after 2-3 days of growth.

Growth of *D. pigrum* directly on BHI agar medium supplemented with triolein and conditioned by growth of nasal *Corynebacterium* species (Table S2). Onto BHI agar supplemented with 200 U/mL of bovine liver catalase (C40-500MG, Sigma) (BHIC), we spread 50 μL of 100 mg/mL of Triolein (BHICT). We then spread 50 μL of a resuspension (OD_{600} of 0.50) of each *Corynebacterium* strain onto a 0.2-μm, 47-mm polycarbonate membrane placed atop 10 mL of BHICT agar in a 100-mm-by-15-mm petri dish. After 2 days, we removed each membrane with *Corynebacterium* cells leaving CFCAM. Using a sterile cotton swab, we then spread either a lawn of *D. pigrum* (from cells resuspended to an OD_{600} of 0.50 in 1x PBS) or *S. pneumoniae* (taken directly from agar medium) onto the CFCAM. Each lawn then grew for 1-2 days before documenting growth or inhibition of growth with digital photography.

Oleic acid disc diffusion assay (Table S3). A lawn of *D. pigrum* or *S. pneumoniae* was spread onto 10 mL of BHIC agar using a sterile cotton swab as described above. Oleic acid (Sigma-Aldrich) was dissolved to a final concentration of 2 mg/mL, 5 mg/mL and 10 mg/mL in ethanol and then we added 10 μl of each to separate, sterile 0.2-μm, 6-mm filter discs (Whatman), with 10 μL of ethanol alone added to a disc as a control. After allowing the solvent to evaporate, filter discs were placed onto the bacterial lawns which were then allowed to grow for 1 day before measuring zones of inhibition and photographing.

***D. pigrum*–*S. aureus* side-by-side coculture assay (Figures 1 and S1).** *D. pigrum* cells were harvested with sterile cotton swabs and resuspended in sterile 1x PBS to a minimal OD_{600} of 0.3 then 5 μl drops were individually inoculated on BHI agar medium and incubated for 2 days. *S. aureus* JE2 was grown overnight on BBL Columbia CNA agar with 5% sheep blood and resuspended in PBS to an OD_{600} of 0.1. Then 5 μl drops of *S. aureus* were inoculated at different distances from the pregrown *D. pigrum*. Inhibition was assessed daily and photographically documented.

Selection of strains and preparation of DNA for whole genome sequencing. *D. pigrum* KPL1914 was isolated from the nostril of a healthy adult (above). In addition, we selected 9 of 27 *D. pigrum* strains from a CDC collection (LaClaire and Facklam, 2000) using an *rpoB*-based typing system with a preference for strains isolated from the nasal passages and/or from children (**Table 1**). Primers Strepto F MOD (AAACTTGGACCAGAAGAAAT) and R MOD (TGTAGCTTATCATCAACCATGTG) were generated *in silico* by mapping primers Strepto F and R (Drancourt et al., 2004) to the *rpoB* sequence of *D. pigrum* ATCC 51524 (genome obtained from NCBI; RefSeq: NZ_AGEF00000000.1) with BLAST (Altschul et al., 1990) and manually correcting misalignments in SnapGene viewer 2.8.2 (GSL Biotech, Chicago, IL). PCR were performed using extracted genomic DNA of *D. pigrum*. PCR conditions were as follows: initial denaturation 95°C for 2 minutes, then 30 cycles of denaturation for 30 seconds at 98°C, annealing

508 at 50°C for 30 seconds, elongation 72°C for minutes and a final extension step at 72°C for 10
509 minutes. PCR products were cleaned using QIAquick PCR purification kit (Qiagen, Germantown,
510 MD) and sequence determined by Sanger sequencing (Macrogen USA, Boston, MA, USA). In the
511 genomic analysis, we also included the publicly available genome for *D. pigrum* ATCC 51524,
512 which was sequenced by the BROAD institute as part of the HMP (RefSeq
513 NZ_AGEF00000000.1).

514 *D. pigrum* strains were grown atop membranes for 48 hrs as described above. Cells were
515 harvested with a sterile tip, resuspended in 50 µl of sterile PBS and frozen at -80°C. Genomic
516 DNA was extracted using the Epicentre MasterPure nucleic acid extraction kit (Epicentre,
517 Madison, WI) per the manufacturer's instructions. We assessed DNA purity using a Nanodrop
518 spectrophotometer (Nanodrop, Wilmington, DE), concentration using Qubit fluorometer
519 (Invitrogen, Carlsbad, CA) and fragment size/quality via agarose gel electrophoresis.

520 **Whole genome sequencing, read assembly and annotation.** Genomic DNA was sequenced
521 at the Yale Center for Genome Analysis (YCGA), New Haven, CT, on an Illumina MiSeq platform
522 using mated paired-end (2 x 250 bp) technology, assembled using de Bruijn graph algorithms
523 with Velvet (Zerbino and Birney, 2008) with a kmer size of 139 bp and annotated with RAST with
524 FIGfam release 70 (Aziz et al., 2008) and Prokka (Seemann, 2014). In addition, *D. pigrum* strains
525 KPL1914 and CDC#4709-98 (LaClaire and Facklam, 2000) were sequenced on a PacBio RS II
526 (Pacific Biosystems, Menlo Park, CA) and sequences were assembled using HGAP version 3.0
527 (Chin et al., 2013). We used an iterative procedure to error correct the PacBio genomes, which
528 involved mapping Illumina reads to the PacBio genomes until there were no differences detected
529 between the Illumina reads and the PacBio assembly (Pettigrew et al., 2018). To estimate the
530 degree of assembly errors and missing content that might contribute to the variation in gene
531 content, we compared the Illumina assembly of KPL1914 with the Illumina-corrected PacBio
532 assembly of KPL1914 to estimate the possible divergence (Hilty et al., 2014). Within Illumina

533 assemblies, we identified 139 (1566 vs. 1705) predicted coding sequences as determined by
534 RAST annotation absent in the assembly received by PacBio sequencing. Genomes were
535 deposited at NCBI (GenBank: NAJJ00000000, NAQW00000000, NAQX00000000,
536 NAQV00000000, NAQU00000000, NAQT00000000, NAQS00000000, NAQR00000000,
537 NAQQ00000000 and NAQP00000000 in BioProjects PRJNA379818 and PRJNA379966).

538 **Identification of the *D. pigrum* core, shell and cloud genome based on Illumina-sequenced**
539 **genomes from 11 strains.** Core proteins from RAST-annotated GenBank-files were determined
540 using the intersection of bidirectional best-hits (BDBH), cluster of orthologous (COG) triangles
541 and Markov Cluster Algorithm (OrthoMCL) clustering algorithms using GET_HOMOLOGUES
542 package version 02012019 on Ubuntu-Linux (Contreras-Moreira and Vinuesa, 2013) excluding
543 proteins with more than one copy in an input species (as single-copy proteins are safer
544 orthologues, i.e., using flag t-11). GenBank files derived from RAST annotation (see above) were
545 renamed with KPL strain names except for strain ATCC51524. As an initial control, amino acid
546 fasta files (*.faa) were used for the determination of core proteins. We determined the cloud, shell
547 and core genome of each of the 11 sequenced *D. pigrum* strains using the
548 parse_pangenome_matrix.pl script (./parse_pangenome_matrix.pl -m
549 sample_intersection/pangenome_matrix_t0.tab -s) of the GET_HOMOLOGUES package version
550 30062017 (Contreras-Moreira and Vinuesa, 2013). Definition of cloud, shell and core genome
551 were based on (Kaas et al., 2012). In brief, cloud is defined as genes only present in a 1 or 2
552 genomes (cut-off is defined as the class next to the most populated non-core cluster class). The
553 core genome is composed of clusters present in all 11 strains, soft core contains clusters present
554 in 10 genomes and shell includes clusters present in 3 to 9 genomes. Synteny analysis on BDBH
555 core (with flag t11) was performed using the compare_clusters script (-s) and synteny
556 visualization was done in MAUVE using standard settings (Darling et al., 2010) after the KPL1914

557 genome was reverse complemented and both genomes had the origin set at the beginning of
558 *dnaA*.

559 **Phylogenetic reconstruction, sequence and protein similarities.** A monophyletic (clade) core
560 genome phylogenic tree was constructed by including *A. otitis* (closest neighbor based on the
561 Living Tree Project (Yarza et al., 2008)) an outgroup (**Figure S6B**). A phylogenic tree without an
562 outgroup was also constructed similarly (**Figure S6A**). *A. otitis* ATCC 51267 contigs were
563 downloaded from NCBI (NZ_AGXA00000000.1) and annotated using RAST (see above).
564 Predicted core proteins common to *A. otitis* and *D. pigrum* genomes were identified as described
565 above using GET_HOMOLOGUES package. Alignments were done using a loop with Clustal
566 Omega V. 1.2.4 ($ for filename in *.faa; do clustalo -i "$filename" -o
567 clustalo_out/${filename%coral} -v; done) and resulting alignments were concatenated using
568 catfasta2phyml perl script (https://github.com/nylander/catfasta2phyml) $./catfasta2phyml.pl *.faa
569 --verbose > outv.phy. PhyML 3.0 (Guindon et al., 2010) with smart model selection (Lefort et al.,
570 2017) using Akaike information criterion was used for phylogenetic analysis (maximum-likelihood)
571 with 100 regular bootstrap replicates and FigTree (http://tree.bio.ed.ac.uk/software/figtree/) for
572 tree visualization.

573 BLAST Ring Image Generator (BRIG) was used for visualization of the other sequenced genomes
574 compared to the closed CDC 4709-98 genome (**Figure S5**) (Alikhan et al., 2011). Average amino
575 acid and nucleic acid identity (**Figure S4**) was calculated using GET_HOMOLOGUES package
576 version 30062017 (Contreras-Moreira and Vinuesa, 2013). In brief, a pangenome matrix was
577 generated using the OMCL algorithm (./get_homologues.pl -d dpig_folder -t 0 -M (OMCL)) for
578 homologues identification. Both, ANI and AAI were calculated with all available clusters (t 0).
579 Commands used: Generation of an AA identity matrix: $ ./get_homologues.pl -d “gbk-files” -A -t
580 0 -M and CDS identity matrix with the command $./get_homologues.pl -d “gbk files” -a 'CDS' -A -
581 t 0 -M.

582 **Measurement of L-Lactic Acid Concentration (Figure 5A).** *D. pigrum* cells were grown from
583 frozen stocks as above. Cells were then harvested with a sterile cotton swab, resuspended to an
584 OD_{600} of 0.50 in 1x PBS and inoculated at 1:25 in BHI broth for overnight growth gently shaking
585 (~50-60 rpm) at 37°C under atmospheric conditions. The overnight culture was then inoculated
586 at 1:25 into fresh BHI broth and grown for 24 hrs at 37°C prior to measuring the lactic acid
587 concentration (mmol/L) using a D-lactic acid/L-lactic acid kit per the manufacturer's instructions
588 (Cat. no. 11112821035, R-Biopharm AG).

589 **Growth of *S. aureus* and *S. pneumoniae* in *D. pigrum* cell-free conditioned liquid medium.**
590 **(**CFCM in **Figures 5B** and **5C**) After growth in BHI, as described for L-lactic acid measurement,
591 *D. pigrum* KPL1914 cells were removed with a 0.22-μM sterile filter yielding cell-free conditioned
592 medium (CFCM). We adjusted the pH of the *D. pigrum* CFCM using 2N H_2SO_4 and 10M KOH to
593 match that of BHI broth alone within 0.02 pH units. *S. aureus* strains Newman and JE2 and *S.*
594 *pneumoniae* strains TIGR4, DBL5, 603, WU2 were each grown on BBL Columbia CNA agar with
595 5% sheep blood for 1 day, harvested with a sterile cotton swab, resuspended to an OD_{600} of 0.30
596 in 1x PBS, inoculated at 1:100 into both *D. pigrum* CFCM and BHI broth and grown for 19-20 hrs
597 at 37°C in shaking (*S. aureus*; 50 rpm) or static (*S. pneumoniae*) culture under atmospheric
598 conditions. Growth yield was quantified as OD_{600} absorbance.

599 **Growth of *S. aureus* and *S. pneumoniae* in BHI broth supplemented with L-lactic acid.**
600 (Lactic Acid in **Figures 5B** and **5C**) Strains of *S. aureus* and *S. pneumoniae* were grown and
601 harvested as described above for inoculation. BHI broth, supplemented with L-lactic acid (CAS
602 no. 79-33-4; Fisher BioReagents) at varying concentrations from 11mM – 55 mM, was sterilized
603 through a 0.22-μM filter. After inoculating each strain separately into BHI broth with L-lactic acid,
604 cultures were grown as described above for growth in CFCM. Growth yield was quantified as
605 OD_{600} absorbance.

Growth assay for *S. pneumoniae* on BHI agar medium conditioned by mono- vs. coculture of *D. pigrum* and/or *C. pseudodiphtheriticum* (Figures 6 and S7). *D. pigrum* and *C. pseudodiphtheriticum* strains were grown from freezer stocks as described above. Cells were harvested with sterile cotton swabs and resuspended in sterile PBS to an OD_{600nm} of 0.5. We then spotted 100 µl of 1:1 mixed resuspension on a polycarbonate membrane (see above) on BHI agar medium containing 400U/mL bovine liver catalase. After 2 days of growth, the polycarbonate membrane with *D. pigrum* and/or *C. pseudodiphtheriticum* was removed from each plate leaving CFCAM. *S. pneumoniae* 603 (Malley et al., 2001) was grown overnight on BBL Columbia CNA agar with 5% sheep blood as described above and, using a sterile cotton swab, a lawn was streaked onto the CFCAM and allowed to grow for 24 hours. Growth/inhibition was assessed daily and photographically recorded. Imaging was difficult due to the transparency of *S. pneumoniae* lawns.

Biosynthetic gene clusters and antibiotic resistance genes (Table S6 and Figure S8). AntiSMASH (antibiotics & Secondary Metabolite Analysis SHell) and ClusterFinder (Medema et al., 2011; Weber et al., 2015) were accessed at https://antismash.secondarymetabolites.org/ using default setpoints. Putative antibiotic resistance genes or mutations in genes conferring antibiotic resistance were predicted using Resistance Gene Identifier (RGI) on the Comprehensive Antibiotic Resistance Database (CARD) (McArthur et al., 2013). Assembly contigs were submitted at RGI (https://card.mcmaster.ca/analyze/rgi) and only perfect and strict hits were allowed. ResFinder version 2.1. (https://cge.cbs.dtu.dk/services/ResFinder/) with 90% threshold for %ID and 60% minimum length (Zankari et al., 2012).

Statistical analyses. Stata version 14.2 (College Station, TX) and R version 3.3.1 using RStudio version 0.99.896 were used for statistical analysis and figure design. A two-tailed *p* value of < 0.05 was considered statistically significant and effect sizes are reported.

630 **Acknowledgments.** We thank Richard R. Facklam and Lynn Shewmaker for providing strains;
631 Joshua Metlay for providing data; Markus Hilty and Stephany Flores Ramos for manuscript edits;
632 and Markus Hilty, Lindsey Bomar, Srikanth Mairpady Shambat, Annelies Zinkernagel and
633 members of the Lemon Lab for helpful discussions.

634 This work was supported by the National Institutes of Health through the National Institute of
635 General Medical Sciences R01 GM117174 (KPL) and the National Institute of Deafness and other
636 Communication Disorders R01 DC013554 (MMP); by the Swiss National Science Foundation and
637 Swiss Foundation for Grants in Biology and Medicine P3SMP3_155315 (SDB); by the Novartis
638 Foundation for Medical-Biological Research 16B065 (SDB); and by the Promedica Foundation
639 1449/M (SDB). Funders had no role in the preparation of this manuscript or decision to publish.

640 **Author contributions.** Conceptualization: SDB, MMP, KPL. Methodology: SDB, SME, MMH.
641 Investigation: SDB, SME, IFE, YK. Interpretation of data: SDB, SME, MMP, IFE, MH, YK, KPL.
642 Visualization: SDB, SME, IFE. Wrote Original Draft: SDB, SME, KPL. Editing and review: SDB,
643 MMP, SME, IFE, KPL. Supervision: SDB, KPL. Funding Acquisition: SDB, MMP, KPL

644 **Declaration of interests.** The authors declare no competing interests.

645 **Table 1. Characteristics of *D. pigrum* strains and Illumina genomes in this study.**

Strain name	Internal reference	Source (citation)	Geography / body site / age	Median fold coverage	CDS[+]	RNAs[+]	GC content (%)[+]	Size (bp)
KPL1914	KPL1914	This study	Massachusetts / nostril / adult	83	1566	72	40	1,726,398
CDC 39-95	KPL1922	CDC (LaClaire and Facklam, 2000)	Canada / sinus / 3 years	62	1666	80	39.7	1,859,258
CDC 2949-98	KPL1930	CDC (LaClaire and Facklam, 2000)	AZ / nasopharyngeal / NA	60	1644	73	39.6	1,886,398
CDC 4294-98	KPL1931	CDC (LaClaire and Facklam, 2000)	SC / blood / 2 months	73	1841	78	39.5	2,014,679
CDC 4420-98	KPL1932	CDC (LaClaire and Facklam, 2000)	TN / blood / 11 years	63	1745	73	39.7	1,934,436
CDC 4545-98	KPL1933	CDC (LaClaire and Facklam, 2000)	AZ / nasopharyngeal / NA	128	1680	61	39.6	1,861,299
CDC 4709-98	KPL1934	CDC (LaClaire and Facklam, 2000)	GA / eye / 2 months	81	1686	80	39.6	1,912,682
CDC 4199-99	KPL1937	CDC (LaClaire and Facklam, 2000)	GA / blood / 1.8 years	107	1746	85	39.6	1,976,602
CDC 4791-99	KPL1938	CDC (LaClaire and Facklam, 2000)	AZ / nasopharyngeal / NA	61	1651	80	39.6	1,873,869
CDC 4792-99	KPL1939	CDC (LaClaire and Facklam, 2000)	AZ / nasopharyngeal / NA	92	1704	80	39.4	1,893,917
SS-1342 (NCFB2967) (ATCC 51524)	NA	BROAD / HMP R91/1468 (Aguirre et al., 1993)	England / spinal cord (autopsy)	200*	1651	31	39.6	1,846,028

646 ***sequenced by the BROAD institute for the Human Microbiota Project**

647 **[+] as determined by RAST annotation (see text)**

648

649 **Table 2: Non-*D. pigrum* bacterial strains used in this stud**

Species	Strain	Internal Reference	Reference	Characteristics
C. accolens	KPL1818	KPL1818	(Bomar et al., 2016)	primary adult human nostril isolate; lipid dependent
C. pseudodiphtheriticum	KPL1989	KPL1989	This study	primary adult human nostril isolate; lipid independent
C. pseudodiphtheriticum	DSM44287^T	KPL2589	(Lehmann and Neumann, 1896)	type strain; lipid independent
C. propinquum	DSM44285^T	KPL1955	(Riegel et al., 1993)	type strain; lipid independent
S. aureus	Newman	KPL2023	(Miller et al., 1977)	lab-adapted strain
S. aureus	JE2	KPL2115	(Fey et al., 2013)	plasmid-free derivative of USA300 LAC
S. pneumoniae	TIGR4	KPL1904	(Tettelin et al., 2001)	Clinical isolate
S. pneumoniae	DBL5	KPL1905	(Lu et al., 2010)	Clinical isolate
S. pneumoniae	603	KPL1906	(Malley et al., 2001)	Clinical isolate
S. pneumoniae	WU2	KPL1907	(Briles et al., 1981)	Clinical isolate

REFERENCES

Aguirre, M., Morrison, D., Cookson, B.D., Gay, F.W., and Collins, M.D. (1993). Phenotypic and phylogenetic characterization of some Gemella-like organisms from human infections: description of Dolosigranulum pigrum gen. nov., sp. nov. J Appl Bacteriol *75*, 608-612.

Alikhan, N.F., Petty, N.K., Ben Zakour, N.L., and Beatson, S.A. (2011). BLAST Ring Image Generator (BRIG): simple prokaryote genome comparisons. BMC Genomics *12*, 402.

Altschul, S.F., Gish, W., Miller, W., Myers, E.W., and Lipman, D.J. (1990). Basic local alignment search tool. J Mol Biol *215*, 403-410.

Aziz, R.K., Bartels, D., Best, A.A., DeJongh, M., Disz, T., Edwards, R.A., Formsma, K., Gerdes, S., Glass, E.M., Kubal, M.*, et al.* (2008). The RAST Server: rapid annotations using subsystems technology. BMC Genomics *9*, 75.

Biesbroek, G., Bosch, A.A., Wang, X., Keijser, B.J., Veenhoven, R.H., Sanders, E.A., and Bogaert, D. (2014a). The impact of breastfeeding on nasopharyngeal microbial communities in infants. American journal of respiratory and critical care medicine *190*, 298-308.

Biesbroek, G., Tsivtsivadze, E., Sanders, E.A., Montijn, R., Veenhoven, R.H., Keijser, B.J., and Bogaert, D. (2014b). Early respiratory microbiota composition determines bacterial succession patterns and respiratory health in children. American journal of respiratory and critical care medicine *190*, 1283-1292.

Bode, L.G., Kluytmans, J.A., Wertheim, H.F., Bogaers, D., Vandenbroucke-Grauls, C.M., Roosendaal, R., Troelstra, A., Box, A.T., Voss, A., van der Tweel, I.*, et al.* (2010). Preventing surgical-site infections in nasal carriers of Staphylococcus aureus. N Engl J Med *362*, 9-17.

Bogaert, D., De Groot, R., and Hermans, P.W. (2004). Streptococcus pneumoniae colonisation: the key to pneumococcal disease. The Lancet infectious diseases *4*, 144-154.

Bogaert, D., Keijser, B., Huse, S., Rossen, J., Veenhoven, R., van Gils, E., Bruin, J., Montijn, R., Bonten, M., and Sanders, E. (2011). Variability and diversity of nasopharyngeal microbiota in children: a metagenomic analysis. PLoS One *6*, e17035.

Bomar, L., Brugger, S.D., and Lemon, K.P. (2018). Bacterial microbiota of the nasal passages across the span of human life. Current opinion in microbiology *41*, 8-14.

Bomar, L., Brugger, S.D., Yost, B.H., Davies, S.S., and Lemon, K.P. (2016). Corynebacterium accolens Releases Antipneumococcal Free Fatty Acids from Human Nostril and Skin Surface Triacylglycerols. MBio *7*, e01725-01715.

Bosch, A., de Steenhuijsen Piters, W.A.A., van Houten, M.A., Chu, M., Biesbroek, G., Kool, J., Pernet, P., de Groot, P.C.M., Eijkemans, M.J.C., Keijser, B.J.F.*, et al.* (2017). Maturation of the Infant Respiratory Microbiota, Environmental Drivers, and Health Consequences. A Prospective Cohort Study. Am J Respir Crit Care Med *196*, 1582-1590.

685 Bosch, A., Levin, E., van Houten, M.A., Hasrat, R., Kalkman, G., Biesbroek, G., de Steenhuijsen
686 Piters, W.A.A., de Groot, P.C.M., Pernet, P., Keijser, B.J.F*., et al.* (2016). Development of Upper
687 Respiratory Tract Microbiota in Infancy is Affected by Mode of Delivery. EBioMedicine *9*, 336-
688 345.

689 Briles, D.E., Nahm, M., Schroer, K., Davie, J., Baker, P., Kearney, J., and Barletta, R. (1981).
690 Antiphosphocholine antibodies found in normal mouse serum are protective against intravenous
691 infection with type 3 streptococcus pneumoniae. J Exp Med *153*, 694-705.

692 Brugger, S.D., Bomar, L., and Lemon, K.P. (2016). Commensal-Pathogen Interactions along the
693 Human Nasal Passages. PLoS pathogens *12*, e1005633.

694 Callahan, B.J., McMurdie, P.J., Rosen, M.J., Han, A.W., Johnson, A.J., and Holmes, S.P.
695 (2016). DADA2: High-resolution sample inference from Illumina amplicon data. Nat Methods *13*,
696 581-583.

697 Camarinha-Silva, A., Jauregui, R., Pieper, D.H., and Wos-Oxley, M.L. (2012a). The temporal
698 dynamics of bacterial communities across human anterior nares. Environ Microbiol Rep *4*, 126-
699 132.

700 Camarinha-Silva, A., Wos-Oxley, M.L., Jauregui, R., Becker, K., and Pieper, D.H. (2012b).
701 Validating T-RFLP as a sensitive and high-throughput approach to assess bacterial diversity
702 patterns in human anterior nares. FEMS Microbiol Ecol *79*, 98-108.

703 Camelo-Castillo, A., Henares, D., Brotons, P., Galiana, A., Rodriguez, J.C., Mira, A., and
704 Munoz-Almagro, C. (2019). Nasopharyngeal Microbiota in Children With Invasive
705 Pneumococcal Disease: Identification of Bacteria With Potential Disease-Promoting and
706 Protective Effects. Front Microbiol *10*, 11.

707 Caporaso, J.G., Bittinger, K., Bushman, F.D., DeSantis, T.Z., Andersen, G.L., and Knight, R.
708 (2010a). PyNAST: a flexible tool for aligning sequences to a template alignment. Bioinformatics
709 *26*, 266-267.

710 Caporaso, J.G., Kuczynski, J., Stombaugh, J., Bittinger, K., Bushman, F.D., Costello, E.K.,
711 Fierer, N., Pena, A.G., Goodrich, J.K., Gordon, J.I*., et al.* (2010b). QIIME allows analysis of
712 high-throughput community sequencing data. Nat Methods *7*, 335-336.

713 Caputo, M., Zoch-Lesniak, B., Karch, A., Vital, M., Meyer, F., Klawonn, F., Baillot, A., Pieper,
714 D.H., and Mikolajczyk, R.T. (2019). Bacterial community structure and effects of picornavirus
715 infection on the anterior nares microbiome in early childhood. BMC Microbiol *19*, 1.

716 Cardenas, N., Martin, V., Arroyo, R., Lopez, M., Carrera, M., Badiola, C., Jimenez, E., and
717 Rodriguez, J.M. (2019). Prevention of Recurrent Acute Otitis Media in Children Through the Use
718 of Lactobacillus salivarius PS7, a Target-Specific Probiotic Strain. Nutrients *11*.

719 Chin, C.S., Alexander, D.H., Marks, P., Klammer, A.A., Drake, J., Heiner, C., Clum, A.,
720 Copeland, A., Huddleston, J., Eichler, E.E*., et al.* (2013). Nonhybrid, finished microbial genome
721 assemblies from long-read SMRT sequencing data. Nat Methods *10*, 563-569.

Chonmaitree, T., Jennings, K., Golovko, G., Khanipov, K., Pimenova, M., Patel, J.A., McCormick, D.P., Loeffelholz, M.J., and Fofanov, Y. (2017). Nasopharyngeal microbiota in infants and changes during viral upper respiratory tract infection and acute otitis media. PLoS One *12*, e0180630.

Claesen, J., Spagnolo, J., Flores Ramos, S., Kurita, K., Byrd, A., Aksenov, I.A., Melnik, A., Wong, W., Wang, S., Hernandez, R.*, et al.* (2019). Cutibacterium acnes antibiotic production shapes niche competition in the human skin microbiome. bioRxiv https://www.biorxiv.org/content/10.1101/594010v1.

Coleman, A., and Cervin, A. (2019). Probiotics in the treatment of otitis media. The past, the present and the future. Int J Pediatr Otorhinolaryngol *116*, 135-140.

Collaborators, G.B.D.L.R.I. (2018). Estimates of the global, regional, and national morbidity, mortality, and aetiologies of lower respiratory infections in 195 countries, 1990-2016: a systematic analysis for the Global Burden of Disease Study 2016. The Lancet infectious diseases *18*, 1191-1210.

Contreras-Moreira, B., and Vinuesa, P. (2013). GET_HOMOLOGUES, a versatile software package for scalable and robust microbial pangenome analysis. Appl Environ Microbiol *79*, 7696-7701.

Copeland, E., Leonard, K., Carney, R., Kong, J., Forer, M., Naidoo, Y., Oliver, B.G.G., Seymour, J.R., Woodcock, S., Burke, C.M.*, et al.* (2018). Chronic Rhinosinusitis: Potential Role of Microbial Dysbiosis and Recommendations for Sampling Sites. Front Cell Infect Microbiol *8*, 57.

Darling, A.E., Mau, B., and Perna, N.T. (2010). progressiveMauve: multiple genome alignment with gene gain, loss and rearrangement. PLoS One *5*, e11147.

De Boeck, I., Wittouck, S., Wuyts, S., Oerlemans, E.F.M., van den Broek, M.F.L., Vandenheuvel, D., Vanderveken, O., and Lebeer, S. (2017). Comparing the Healthy Nose and Nasopharynx Microbiota Reveals Continuity As Well As Niche-Specificity. Front Microbiol *8*, 2372.

de Steenhuijsen Piters, W.A., and Bogaert, D. (2016). Unraveling the Molecular Mechanisms Underlying the Nasopharyngeal Bacterial Community Structure. MBio *7*.

Dong, S.H., Tang, W., Lukk, T., Yu, Y., Nair, S.K., and van der Donk, W.A. (2015). The enterococcal cytolysin synthetase has an unanticipated lipid kinase fold. Elife *4*.

Drancourt, M., Roux, V., Fournier, P.E., and Raoult, D. (2004). rpoB gene sequence-based identification of aerobic Gram-positive cocci of the genera Streptococcus, Enterococcus, Gemella, Abiotrophia, and Granulicatella. J Clin Microbiol *42*, 497-504.

Edgar, R.C. (2010). Search and clustering orders of magnitude faster than BLAST. Bioinformatics *26*, 2460-2461.

Edgar, R.C., Haas, B.J., Clemente, J.C., Quince, C., and Knight, R. (2011). UCHIME improves sensitivity and speed of chimera detection. Bioinformatics *27*, 2194-2200.

Eren, A.M., Morrison, H.G., Lescault, P.J., Reveillaud, J., Vineis, J.H., and Sogin, M.L. (2015). Minimum entropy decomposition: unsupervised oligotyping for sensitive partitioning of high-throughput marker gene sequences. The ISME journal *9*, 968-979.

Escapa, I.F., Chen, T., Huang, Y., Gajare, P., Dewhirst, F.E., and Lemon, K.P. (2018). New Insights into Human Nostril Microbiome from the Expanded Human Oral Microbiome Database (eHOMD): a Resource for the Microbiome of the Human Aerodigestive Tract. mSystems *3*.

Esposito, S., and Principi, N. (2018). Impact of nasopharyngeal microbiota on the development of respiratory tract diseases. Eur J Clin Microbiol Infect Dis *37*, 1-7.

Fey, P.D., Endres, J.L., Yajjala, V.K., Widhelm, T.J., Boissy, R.J., Bose, J.L., and Bayles, K.W. (2013). A genetic resource for rapid and comprehensive phenotype screening of nonessential *Staphylococcus aureus* genes. MBio *4*, e00537-00512.

Fritz, S.A., Hogan, P.G., Hayek, G., Eisenstein, K.A., Rodriguez, M., Epplin, E.K., Garbutt, J., and Fraser, V.J. (2012). Household versus individual approaches to eradication of community-associated Staphylococcus aureus in children: a randomized trial. Clinical infectious diseases : an official publication of the Infectious Diseases Society of America *54*, 743-751.

Galac, M.R., Stam, J., Maybank, R., Hinkle, M., Mack, D., Rohde, H., Roth, A.L., and Fey, P.D. (2017). Complete Genome Sequence of Staphylococcus epidermidis 1457. Genome Announc *5*.

Gan, W., Yang, F., Tang, Y., Zhou, D., Qing, D., Hu, J., Liu, S., Liu, F., and Meng, J. (2019). The difference in nasal bacterial microbiome diversity between chronic rhinosinusitis patients with polyps and a control population. Int Forum Allergy Rhinol.

Guindon, S., Dufayard, J.F., Lefort, V., Anisimova, M., Hordijk, W., and Gascuel, O. (2010). New algorithms and methods to estimate maximum-likelihood phylogenies: assessing the performance of PhyML 3.0. Syst Biol *59*, 307-321.

Haas, W., Gearinger, L.S., Hesje, C.K., Sanfilippo, C.M., and Morris, T.W. (2012). Microbiological etiology and susceptibility of bacterial conjunctivitis isolates from clinical trials with ophthalmic, twice-daily besifloxacin. Adv Ther *29*, 442-455.

Hall, G.S., Gordon, S., Schroeder, S., Smith, K., Anthony, K., and Procop, G.W. (2001). Case of synovitis potentially caused by Dolosigranulum pigrum. J Clin Microbiol *39*, 1202-1203.

Hardy, B.L., Dickey, S.W., Plaut, R.D., Riggins, D.P., Stibitz, S., Otto, M., and Merrell, D.S. (2019). Corynebacterium pseudodiphtheriticum Exploits Staphylococcus aureus Virulence Components in a Novel Polymicrobial Defense Strategy. MBio *10*.

Hasegawa, K., Linnemann, R.W., Mansbach, J.M., Ajami, N.J., Espinola, J.A., Petrosino, J.F., Piedra, P.A., Stevenson, M.D., Sullivan, A.F., Thompson, A.D.*, et al.* (2017). Nasal Airway

793 Microbiota Profile and Severe Bronchiolitis in Infants: A Case-control Study. Pediatr Infect Dis J
794 *36*, 1044-1051.

795 Hilty, M., Wuthrich, D., Salter, S.J., Engel, H., Campbell, S., Sa-Leao, R., de Lencastre, H.,
796 Hermans, P., Sadowy, E., Turner, P.*, et al.* (2014). Global phylogenomic analysis of
797 nonencapsulated Streptococcus pneumoniae reveals a deep-branching classic lineage that is
798 distinct from multiple sporadic lineages. Genome Biol Evol *6*, 3281-3294.

799 Hoedemaekers, A., Schulin, T., Tonk, B., Melchers, W.J., and Sturm, P.D. (2006). Ventilator-
800 associated pneumonia caused by Dolosigranulum pigrum. J Clin Microbiol *44*, 3461-3462.

801 Iwase, T., Uehara, Y., Shinji, H., Tajima, A., Seo, H., Takada, K., Agata, T., and Mizunoe, Y.
802 (2010). Staphylococcus epidermidis Esp inhibits Staphylococcus aureus biofilm formation and
803 nasal colonization. Nature *465*, 346-349.

804 Janek, D., Zipperer, A., Kulik, A., Krismer, B., and Peschel, A. (2016). High Frequency and
805 Diversity of Antimicrobial Activities Produced by Nasal Staphylococcus Strains against Bacterial
806 Competitors. PLoS Pathog *12*, e1005812.

807 Johnsen, B.O., Ronning, E.J., Onken, A., Figved, W., and Jenum, P.A. (2011). Dolosigranulum
808 pigrum causing biomaterial-associated arthritis. APMIS *119*, 85-87.

809 Kaas, R.S., Friis, C., Ussery, D.W., and Aarestrup, F.M. (2012). Estimating variation within the
810 genes and inferring the phylogeny of 186 sequenced diverse Escherichia coli genomes. BMC
811 Genomics *13*, 577.

812 Kandler, O. (1983). Carbohydrate metabolism in lactic acid bacteria. Antonie Van Leeuwenhoek
813 *49*, 209-224.

814 Kelly, M.S., Surette, M.G., Smieja, M., Pernica, J.M., Rossi, L., Luinstra, K., Steenhoff, A.P.,
815 Feemster, K.A., Goldfarb, D.M., Arscott-Mills, T.*, et al.* (2017). The Nasopharyngeal Microbiota
816 of Children With Respiratory Infections in Botswana. Pediatr Infect Dis J *36*, e211-e218.

817 Kluytmans, J., van Belkum, A., and Verbrugh, H. (1997). Nasal carriage of *Staphylococcus*
818 *aureus*: epidemiology, underlying mechanisms, and associated risks. Clinical microbiology
819 reviews *10*, 505-520.

820 Krismer, B., Liebeke, M., Janek, D., Nega, M., Rautenberg, M., Hornig, G., Unger, C.,
821 Weidenmaier, C., Lalk, M., and Peschel, A. (2014). Nutrient limitation governs Staphylococcus
822 aureus metabolism and niche adaptation in the human nose. PLoS Pathog *10*, e1003862.

823 Krismer, B., Weidenmaier, C., Zipperer, A., and Peschel, A. (2017). The commensal lifestyle of
824 Staphylococcus aureus and its interactions with the nasal microbiota. Nature reviews *15*, 675-
825 687.

826 LaClaire, L., and Facklam, R. (2000). Antimicrobial susceptibility and clinical sources of
827 Dolosigranulum pigrum cultures. Antimicrob Agents Chemother *44*, 2001-2003.

828 Langevin, S., Pichon, M., Smith, E., Morrison, J., Bent, Z., Green, R., Barker, K., Solberg, O.,
829 Gillet, Y., Javouhey, E.*, et al.* (2017). Early nasopharyngeal microbial signature associated with
830 severe influenza in children: a retrospective pilot study. J Gen Virol *98*, 2425-2437.

831 Lappan, R., Imbrogno, K., Sikazwe, C., Anderson, D., Mok, D., Coates, H., Vijayasekaran, S.,
832 Bumbak, P., Blyth, C.C., Jamieson, S.E.*, et al.* (2018). A microbiome case-control study of
833 recurrent acute otitis media identified potentially protective bacterial genera. BMC Microbiol *18*,
834 13.

835 Laufer, A.S., Metlay, J.P., Gent, J.F., Fennie, K.P., Kong, Y., and Pettigrew, M.M. (2011).
836 Microbial communities of the upper respiratory tract and otitis media in children. MBio *2*,
837 e00245-00210.

838 Lecuyer, H., Audibert, J., Bobigny, A., Eckert, C., Janniere-Nartey, C., Buu-Hoi, A., Mainardi,
839 J.L., and Podglajen, I. (2007). Dolosigranulum pigrum causing nosocomial pneumonia and
840 septicemia. J Clin Microbiol *45*, 3474-3475.

841 Lefort, V., Longueville, J.E., and Gascuel, O. (2017). SMS: Smart Model Selection in PhyML.
842 Mol Biol Evol *34*, 2422-2424.

843 Lehmann, K.B., and Neumann, R.O. (1896). Corynebacterium pseudodiphtheriticum. In Atlas
844 und Grundriss der Bakteriologie und Lehrbuch der Speziellen Bakteriologischen Diagnostik
845 (Munich: J.F. Lehmann), pp. 571-572.

846 Lemon, K.P., Klepac-Ceraj, V., Schiffer, H.K., Brodie, E.L., Lynch, S.V., and Kolter, R. (2010).
847 Comparative analyses of the bacterial microbiota of the human nostril and oropharynx. MBio *1*,
848 e00129-00110

849 Lexau, C.A., Lynfield, R., Danila, R., Pilishvili, T., Facklam, R., Farley, M.M., Harrison, L.H.,
850 Schaffner, W., Reingold, A., Bennett, N.M.*, et al.* (2005). Changing epidemiology of invasive
851 pneumococcal disease among older adults in the era of pediatric pneumococcal conjugate
852 vaccine. JAMA *294*, 2043-2051.

853 Lin, J.C., Hou, S.J., Huang, L.U., Sun, J.R., Chang, W.K., and Lu, J.J. (2006). Acute
854 cholecystitis accompanied by acute pancreatitis potentially caused by Dolosigranulum pigrum. J
855 Clin Microbiol *44*, 2298-2299.

856 Liu, C.M., Price, L.B., Hungate, B.A., Abraham, A.G., Larsen, L.A., Christensen, K., Stegger, M.,
857 Skov, R., and Andersen, P.S. (2015). Staphylococcus aureus and the ecology of the nasal
858 microbiome. Sci Adv *1*, e1400216.

859 Lu, Y.J., Leite, L., Goncalves, V.M., Dias Wde, O., Liberman, C., Fratelli, F., Alderson, M., Tate,
860 A., Maisonneuve, J.F., Robertson, G.*, et al.* (2010). GMP-grade pneumococcal whole-cell
861 vaccine injected subcutaneously protects mice from nasopharyngeal colonization and fatal
862 aspiration-sepsis. Vaccine *28*, 7468-7475.

863 Luna, P.N., Hasegawa, K., Ajami, N.J., Espinola, J.A., Henke, D.M., Petrosino, J.F., Piedra,
864 P.A., Sullivan, A.F., Camargo, C.A., Jr., Shaw, C.A.*, et al.* (2018). The association between

anterior nares and nasopharyngeal microbiota in infants hospitalized for bronchiolitis. Microbiome *6*, 2.

Malley, R., Lipsitch, M., Stack, A., Saladino, R., Fleisher, G., Pelton, S., Thompson, C., Briles, D., and Anderson, P. (2001). Intranasal immunization with killed unencapsulated whole cells prevents colonization and invasive disease by capsulated pneumococci. Infect Immun *69*, 4870-4873.

Man, W.H., Clerc, M., de Steenhuijsen Piters, W.A.A., van Houten, M.A., Chu, M., Kool, J., Keijser, B.J.F., Sanders, E.A.M., and Bogaert, D. (2019a). Loss of Microbial Topography between Oral and Nasopharyngeal Microbiota and Development of Respiratory Infections Early in Life. Am J Respir Crit Care Med.

Man, W.H., de Steenhuijsen Piters, W.A., and Bogaert, D. (2017). The microbiota of the respiratory tract: gatekeeper to respiratory health. Nature reviews *15*, 259-270.

Man, W.H., van Houten, M.A., Merelle, M.E., Vlieger, A.M., Chu, M., Jansen, N.J.G., Sanders, E.A.M., and Bogaert, D. (2019b). Bacterial and viral respiratory tract microbiota and host characteristics in children with lower respiratory tract infections: a matched case-control study. Lancet Respir Med *7*, 417-426.

Mandal, S., Van Treuren, W., White, R.A., Eggesbo, M., Knight, R., and Peddada, S.D. (2015). Analysis of composition of microbiomes: a novel method for studying microbial composition. Microb Ecol Health Dis *26*, 27663.

Manning, J., Dunne, E.M., Wescombe, P.A., Hale, J.D., Mulholland, E.K., Tagg, J.R., Robins-Browne, R.M., and Satzke, C. (2016). Investigation of Streptococcus salivarius-mediated inhibition of pneumococcal adherence to pharyngeal epithelial cells. BMC Microbiol *16*, 225.

McArthur, A.G., Waglechner, N., Nizam, F., Yan, A., Azad, M.A., Baylay, A.J., Bhullar, K., Canova, M.J., De Pascale, G., Ejim, L.*, et al.* (2013). The comprehensive antibiotic resistance database. Antimicrob Agents Chemother *57*, 3348-3357.

Medema, M.H., Blin, K., Cimermancic, P., de Jager, V., Zakrzewski, P., Fischbach, M.A., Weber, T., Takano, E., and Breitling, R. (2011). antiSMASH: rapid identification, annotation and analysis of secondary metabolite biosynthesis gene clusters in bacterial and fungal genome sequences. Nucleic acids research *39*, W339-346.

Miller, K.D., Hetrick, D.L., and Bielefeldt, D.J. (1977). Production and properties of *Staphylococcus aureus* (strain Newman D2C) with uniform clumping factor activity. Thromb Res *10*, 203-211.

Nakatsuji, T., Chen, T.H., Narala, S., Chun, K.A., Two, A.M., Yun, T., Shafiq, F., Kotol, P.F., Bouslimani, A., Melnik, A.V.*, et al.* (2017). Antimicrobials from human skin commensal bacteria protect against Staphylococcus aureus and are deficient in atopic dermatitis. Sci Transl Med *9*.

O'Sullivan, J.N., Rea, M.C., O'Connor, P.M., Hill, C., and Ross, R.P. (2019). Human skin microbiota is a rich source of bacteriocin-producing staphylococci that kill human pathogens. FEMS Microbiol Ecol *95*.

Otto, M., Echner, H., Voelter, W., and Gotz, F. (2001). Pheromone cross-inhibition between Staphylococcus aureus and Staphylococcus epidermidis. Infect Immun *69*, 1957-1960.

Otto, M., Sussmuth, R., Vuong, C., Jung, G., and Gotz, F. (1999). Inhibition of virulence factor expression in Staphylococcus aureus by the Staphylococcus epidermidis agr pheromone and derivatives. FEBS Lett *450*, 257-262.

Paharik, A.E., Parlet, C.P., Chung, N., Todd, D.A., Rodriguez, E.I., Van Dyke, M.J., Cech, N.B., and Horswill, A.R. (2017). Coagulase-Negative Staphylococcal Strain Prevents Staphylococcus aureus Colonization and Skin Infection by Blocking Quorum Sensing. Cell Host Microbe *22*, 746-756 e745.

Parlet, C.P., Brown, M.M., and Horswill, A.R. (2019). Commensal Staphylococci Influence Staphylococcus aureus Skin Colonization and Disease. Trends Microbiol *27*, 497-507.

Perez-Losada, M., Alamri, L., Crandall, K.A., and Freishtat, R.J. (2017). Nasopharyngeal Microbiome Diversity Changes over Time in Children with Asthma. PLoS One *12*, e0170543.

Peterson, S.W., Knox, N.C., Golding, G.R., Tyler, S.D., Tyler, A.D., Mabon, P., Embree, J.E., Fleming, F., Fanella, S., Van Domselaar, G.*, et al.* (2016). A Study of the Infant Nasal Microbiome Development over the First Year of Life and in Relation to Their Primary Adult Caregivers Using cpn60 Universal Target (UT) as a Phylogenetic Marker. PLoS One *11*, e0152493.

Pettigrew, M.M., Ahearn, C.P., Gent, J.F., Kong, Y., Gallo, M.C., Munro, J.B., D'Mello, A., Sethi, S., Tettelin, H., and Murphy, T.F. (2018). Haemophilus influenzae genome evolution during persistence in the human airways in chronic obstructive pulmonary disease. Proc Natl Acad Sci U S A *115*, E3256-E3265.

Pettigrew, M.M., Laufer, A.S., Gent, J.F., Kong, Y., Fennie, K.P., and Metlay, J.P. (2012). Upper respiratory tract microbial communities, acute otitis media pathogens, and antibiotic use in healthy and sick children. Appl Environ Microbiol *78*, 6262-6270.

Pfeiler, E.A., and Klaenhammer, T.R. (2007). The genomics of lactic acid bacteria. Trends Microbiol *15*, 546-553.

Piewngam, P., Zheng, Y., Nguyen, T.H., Dickey, S.W., Joo, H.S., Villaruz, A.E., Glose, K.A., Fisher, E.L., Hunt, R.L., Li, B.*, et al.* (2018). Pathogen elimination by probiotic Bacillus via signalling interference. Nature *562*, 532-537.

Ramsey, M.M., Freire, M.O., Gabrilska, R.A., Rumbaugh, K.P., and Lemon, K.P. (2016). Staphylococcus aureus Shifts toward Commensalism in Response to Corynebacterium Species. Front Microbiol *7*, 1230.

936 Repka, L.M., Chekan, J.R., Nair, S.K., and van der Donk, W.A. (2017). Mechanistic
937 Understanding of Lanthipeptide Biosynthetic Enzymes. Chemical reviews *117*, 5457-5520.

938 Riegel, P., de Briel, D., Prevost, G., Jehl, F., and Monteil, H. (1993). Proposal of
939 *Corynebacterium propinquum* sp. nov. for *Corynebacterium* group ANF-3 strains. FEMS
940 Microbiology Letters *113*, 229-234.

941 Sakwinska, O., Bastic Schmid, V., Berger, B., Bruttin, A., Keitel, K., Lepage, M., Moine, D.,
942 Ngom Bru, C., Brussow, H., and Gervaix, A. (2014). Nasopharyngeal microbiota in healthy
943 children and pneumonia patients. J Clin Microbiol *52*, 1590-1594.

944 Salter, S.J., Turner, C., Watthanaworawit, W., de Goffau, M.C., Wagner, J., Parkhill, J., Bentley,
945 S.D., Goldblatt, D., Nosten, F., and Turner, P. (2017). A longitudinal study of the infant
946 nasopharyngeal microbiota: The effects of age, illness and antibiotic use in a cohort of South
947 East Asian children. PLoS Negl Trop Dis *11*, e0005975.

948 Sampo, M., Ghazouani, O., Cadiou, D., Trichet, E., Hoffart, L., and Drancourt, M. (2013).
949 Dolosigranulum pigrum keratitis: a three-case series. BMC Ophthalmol *13*, 31.

950 Schulfer, A., and Blaser, M.J. (2015). Risks of Antibiotic Exposures Early in Life on the
951 Developing Microbiome. PLoS Pathog *11*, e1004903.

952 Seemann, T. (2014). Prokka: rapid prokaryotic genome annotation. Bioinformatics *30*, 2068-
953 2069.

954 Song, C., Chorath, J., Pak, Y., and Redjal, N. (2019). Use of Dipstick Assay and Rapid PCR-
955 DNA Analysis of Nasal Secretions for Diagnosis of Bacterial Sinusitis in Children With Chronic
956 Cough. Allergy Rhinol (Providence) *10*, 2152656718821281.

957 Stubbendieck, R.M., May, D.S., Chevrette, M.G., Temkin, M.I., Wendt-Pienkowski, E.,
958 Cagnazzo, J., Carlson, C.M., Gern, J.E., and Currie, C.R. (2019). Competition among Nasal
959 Bacteria Suggests a Role for Siderophore-Mediated Interactions in Shaping the Human Nasal
960 Microbiota. Appl Environ Microbiol *85*.

961 Suzuki, H., Lefebure, T., Bitar, P.P., and Stanhope, M.J. (2012). Comparative genomic analysis
962 of the genus Staphylococcus including Staphylococcus aureus and its newly described sister
963 species Staphylococcus simiae. BMC Genomics *13*, 38.

964 Tano, K., Hakansson, E.G., Holm, S.E., and Hellstrom, S. (2002). Bacterial interference
965 between pathogens in otitis media and alpha-haemolytic Streptococci analysed in an in vitro
966 model. Acta Otolaryngol *122*, 78-85.

967 Teo, S.M., Mok, D., Pham, K., Kusel, M., Serralha, M., Troy, N., Holt, B.J., Hales, B.J., Walker,
968 M.L., Hollams, E.*, et al.* (2015). The infant nasopharyngeal microbiome impacts severity of
969 lower respiratory infection and risk of asthma development. Cell Host Microbe *17*, 704-715.

970 Tettelin, H., Nelson, K.E., Paulsen, I.T., Eisen, J.A., Read, T.D., Peterson, S., Heidelberg, J.,
971 DeBoy, R.T., Haft, D.H., Dodson, R.J., *et al.* (2001). Complete genome sequence of a virulent
972 isolate of Streptococcus pneumoniae. Science *293*, 498-506.

973 Toivonen, L., Hasegawa, K., Waris, M., Ajami, N.J., Petrosino, J.F., Camargo, C.A., Jr., and
974 Peltola, V. (2019). Early nasal microbiota and acute respiratory infections during the first years
975 of life. Thorax *74*, 592-599.

976 Tong, S.Y., Davis, J.S., Eichenberger, E., Holland, T.L., and Fowler, V.G., Jr. (2015).
977 Staphylococcus aureus infections: epidemiology, pathophysiology, clinical manifestations, and
978 management. Clinical microbiology reviews *28*, 603-661.

979 Turner, N.A., Sharma-Kuinkel, B.K., Maskarinec, S.A., Eichenberger, E.M., Shah, P.P.,
980 Carugati, M., Holland, T.L., and Fowler, V.G., Jr. (2019). Methicillin-resistant Staphylococcus
981 aureus: an overview of basic and clinical research. Nature reviews *17*, 203-218.

982 Venkateswaran, N., Kalsow, C.M., and Hindman, H.B. (2014). Phlyctenular keratoconjunctivitis
983 associated with Dolosigranulum pigrum. Ocul Immunol Inflamm *22*, 242-245.

984 von Eiff, C., Becker, K., Machka, K., Stammer, H., Peters, G., and Group, F.t.S. (2001). Nasal
985 carriage as a source of *Staphylococcus aureus* bacteremia. N Engl J Med *344*, 11-16.

986 Wahl, B., O'Brien, K.L., Greenbaum, A., Majumder, A., Liu, L., Chu, Y., Luksic, I., Nair, H.,
987 McAllister, D.A., Campbell, H., *et al.* (2018). Burden of Streptococcus pneumoniae and
988 Haemophilus influenzae type b disease in children in the era of conjugate vaccines: global,
989 regional, and national estimates for 2000-15. Lancet Glob Health *6*, e744-e757.

990 Walker, R.E., Walker, C.G., Camargo, C.A., Jr., Bartley, J., Flint, D., Thompson, J.M.D., and
991 Mitchell, E.A. (2019). Nasal microbial composition and chronic otitis media with effusion: A
992 case-control study. PLoS One *14*, e0212473.

993 Wang, Q., Garrity, G.M., Tiedje, J.M., and Cole, J.R. (2007). Naive Bayesian classifier for rapid
994 assignment of rRNA sequences into the new bacterial taxonomy. Appl Environ Microbiol *73*,
995 5261-5267.

996 Weber, T., Blin, K., Duddela, S., Krug, D., Kim, H.U., Bruccoleri, R., Lee, S.Y., Fischbach, M.A.,
997 Muller, R., Wohlleben, W., *et al.* (2015). antiSMASH 3.0-a comprehensive resource for the
998 genome mining of biosynthetic gene clusters. Nucleic Acids Res *43*, W237-243.

999 Wen, Z., Xie, G., Zhou, Q., Qiu, C., Li, J., Hu, Q., Dai, W., Li, D., Zheng, Y., and Wen, F. (2018).
1000 Distinct Nasopharyngeal and Oropharyngeal Microbiota of Children with Influenza A Virus
1001 Compared with Healthy Children. Biomed Res Int *2018*, 6362716.

1002 Wertheim, H.F., Vos, M.C., Ott, A., van Belkum, A., Voss, A., Kluytmans, J.A., van Keulen, P.H.,
1003 Vandenbroucke-Grauls, C.M., Meester, M.H., and Verbrugh, H.A. (2004). Risk and outcome of
1004 nosocomial *Staphylococcus aureus* bacteraemia in nasal carriers versus non-carriers. Lancet
1005 *364*, 703-705.

1006 WHO (2012). Pneumococcal vaccines WHO position paper - 2012 - recommendations. Vaccine
1007 *30*, 4717-4718.

1008 Williams, M.R., Costa, S.K., Zaramela, L.S., Khalil, S., Todd, D.A., Winter, H.L., Sanford, J.A.,
1009 O'Neill, A.M., Liggins, M.C., Nakatsuji, T.*, et al.* (2019). Quorum sensing between bacterial
1010 species on the skin protects against epidermal injury in atopic dermatitis. Sci Transl Med *11*.

1011 Wos-Oxley, M.L., Plumeier, I., von Eiff, C., Taudien, S., Platzer, M., Vilchez-Vargas, R., Becker,
1012 K., and Pieper, D.H. (2010). A poke into the diversity and associations within human anterior
1013 nare microbial communities. ISME J *4*, 839-851.

1014 Yan, M., Pamp, S.J., Fukuyama, J., Hwang, P.H., Cho, D.Y., Holmes, S., and Relman, D.A.
1015 (2013). Nasal microenvironments and interspecific interactions influence nasal microbiota
1016 complexity and S. aureus carriage. Cell host & microbe *14*, 631-640.

1017 Yarza, P., Richter, M., Peplies, J., Euzeby, J., Amann, R., Schleifer, K.H., Ludwig, W., Glockner,
1018 F.O., and Rossello-Mora, R. (2008). The All-Species Living Tree project: a 16S rRNA-based
1019 phylogenetic tree of all sequenced type strains. Syst Appl Microbiol *31*, 241-250.

1020 Young, B.C., Wu, C.H., Gordon, N.C., Cole, K., Price, J.R., Liu, E., Sheppard, A.E., Perera, S.,
1021 Charlesworth, J., Golubchik, T.*, et al.* (2017). Severe infections emerge from commensal
1022 bacteria by adaptive evolution. Elife *6*.

1023 Zankari, E., Hasman, H., Cosentino, S., Vestergaard, M., Rasmussen, S., Lund, O., Aarestrup,
1024 F.M., and Larsen, M.V. (2012). Identification of acquired antimicrobial resistance genes. The
1025 Journal of antimicrobial chemotherapy *67*, 2640-2644.

1026 Zerbino, D.R., and Birney, E. (2008). Velvet: algorithms for de novo short read assembly using
1027 de Bruijn graphs. Genome Res *18*, 821-829.

1028 Zhang, M., Wang, R., Liao, Y., Buijs, M.J., and Li, J. (2016). Profiling of Oral and Nasal
1029 Microbiome in Children With Cleft Palate. Cleft Palate Craniofac J *53*, 332-338.

1030 Zipperer, A., Konnerth, M.C., Laux, C., Berscheid, A., Janek, D., Weidenmaier, C., Burian, M.,
1031 Schilling, N.A., Slavetinsky, C., Marschal, M.*, et al.* (2016). Human commensals producing a
1032 novel antibiotic impair pathogen colonization. Nature *535*, 511-516.

1033

Figures

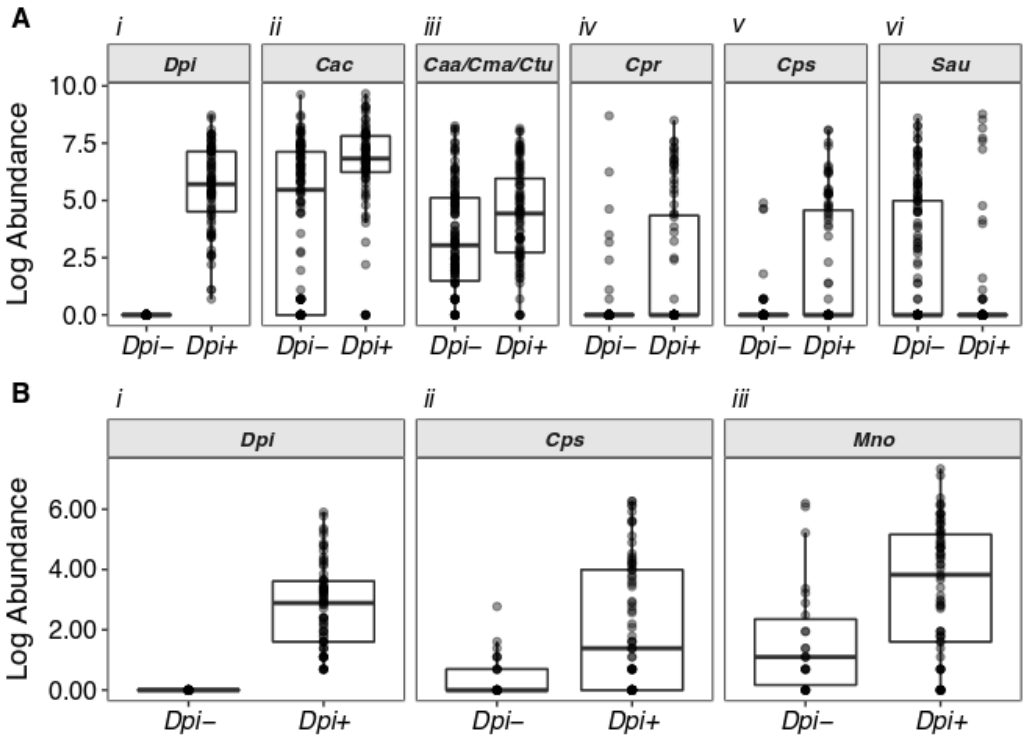

Figure 1. Individual nasal *Corynebacterium* species exhibit increased differential relative abundance in the presence of *D. pigrum* in human nostril microbiota. We used ANCOM to compare species/supraspecies-level composition of 16S rRNA gene nostril datasets from (**A**) 210 adults and (**B**) 99 children ages 6 and 78 months when *D. pigrum* was either absent (Dpi-) or present (Dpi+). Plots show statistically significant findings after correction for multiple testing within ANCOM. The dark bar represents the median; lower and upper hinges correspond to the first and third quartiles. Each gray dot represents the value for a sample, and multiple overlapping dots appear black. Dpi = *Dolosigranulum pigrum*, Cac = *Corynebacterium accolens*, Caa/Cma/Ctu= supraspecies *Corynebacterium accolens_macginleyi_tuberculostearicum*, Cpr = *Corynebacterium propinquum*, Cps = *Corynebacterium pseudodiphtheriticum*, Mno = *Moraxella nonliquefaciens.*

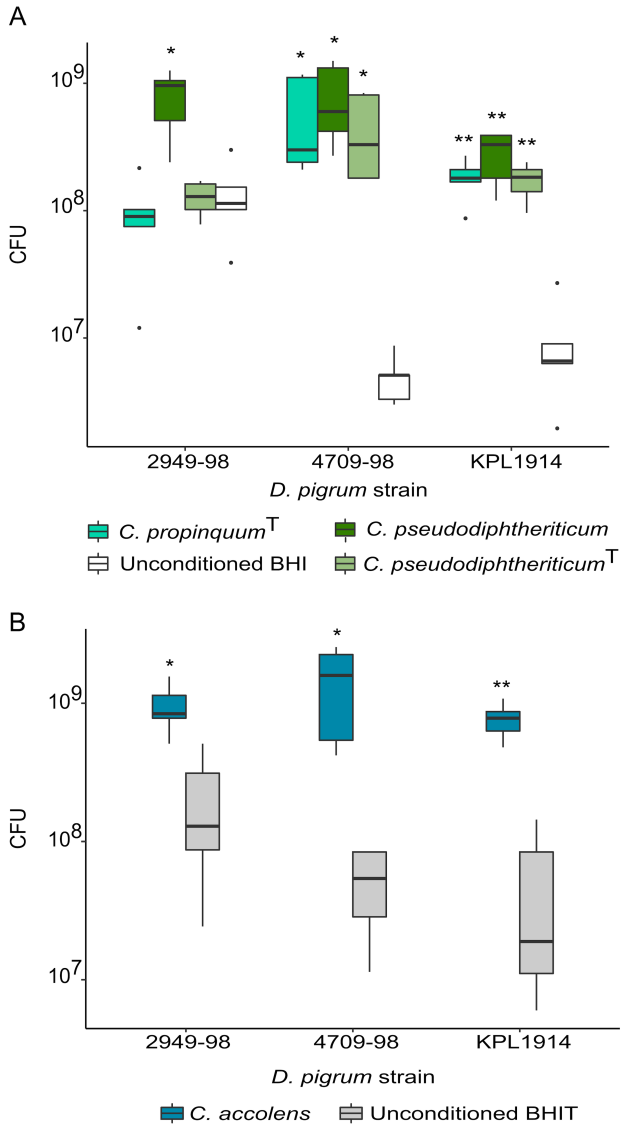

Figure 2. *D. pigrum* growth yields increase on cell-free conditioned agar medium from nasal *Corynebacterium* species. Growth yield of *D. pigrum* strains CDC 2949-98, CDC 4709-98 and KPL1914 was quantified as the number of CFUs grown on a polycarbonate membrane placed onto (**A**) cell-free conditioned BHI agar from *C. propinquum* (aqua green) or *C. pseudodiphtheriticum* (light and dark green) or (**B**) cell-free conditioned BHI-Triolein (BHIT) agar from *C. accolens* (blue) and compared to growth on unconditioned BHI agar (white) or unconditioned BHIT agar (grey), respectively. Data were analyzed separately for each *D. pigrum*

22 strain. CFU counts for each condition were compared to the unconditioned medium (n=5) using

23 a pairwise t test with Bonferroni correction for multiple comparisons. *, $p \leq 0.05$; **, $p \leq 0.001$

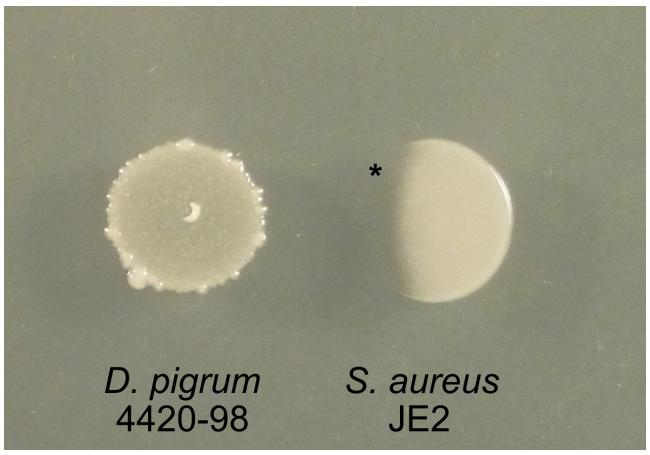

Figure 3. *D. pigrum* inhibits methicillin-resistant *S. aureus* USA300. A pregrown *D. pigrum* CDC 4420-98 inoculum produced a diffusible activity that inhibited the growth of *S. aureus* strain JE2 on BHI agar (*n*=3). A representative image of CDC 4420-98 inhibiting (asterisk) *S. aureus* JE2 is shown (48 hrs). Images of eight additional *D. pigrum* strains inhibiting *S. aureus* are in Figure S1.

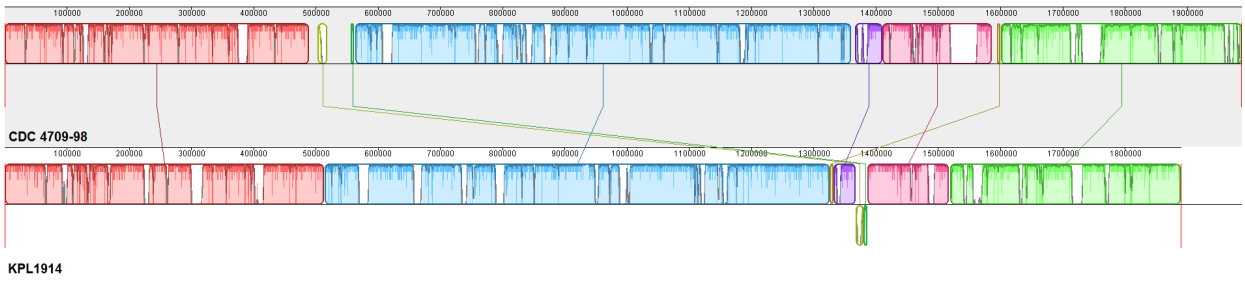

Figure 4. Comparative analysis of two *D. pigrum* genomes reveals a high degree of synteny. Multiple genome alignment for synteny analysis of the two closed *D. pigrum* genomes CDC 4709-98 and KPL1914 was performed using MAUVE (Darling et al., 2010). Locally collinear blocks and similarity profiles are presented, and genome boundaries are indicated (red bar after non-aligned sequences, i.e., sequences that are unique for the corresponding genome).

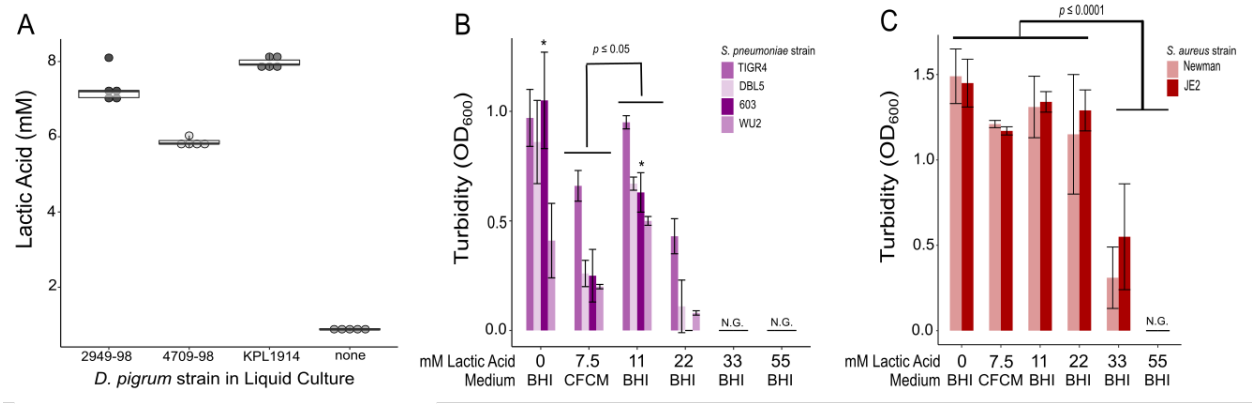

Figure 5. Lactate production by *D. pigrum* is insufficient to inhibit pathobiont growth. Strains of *S. pneumoniae* and *S. aureus* grew in the presence of higher levels of L-lactic acid than those produced by *D. pigrum in vitro*. (**A**) The concentration of L-lactic acid (mM) produced by three *D. pigrum* strains was measured after 24 hrs of gentle shaken aerobic growth in BHI broth at 37°C (n=5) as compared to the basal concentration of L-lactic acid in BHI alone (none). (**B**) The average growth (OD_{600}) of 4 *S. pneumoniae* strains in *D. pigrum* KPL1914 CFCM or in unconditioned BHI broth supplemented with different concentrations of L-lactic acid measured after 19–20 hrs of static aerobic growth at 37°C (n=4). (C) The average growth (OD_{600}) of 2 *S. aureus* strains in *D. pigrum* KPL1914 CFCM or in unconditioned BHI broth supplemented with different concentrations of L-lactic acid measured after 19–20 hrs of shaken aerobic growth at 37°C (n=4). Average growth of *S. pneumoniae* in BHI, CFCM and 11 mM L-lactic acid and of *S. aureus* in all conditions were analyzed for each individual strain using an ANOVA and Tukey's HSD test for multiple comparisons. * indicates $p \leq 0.05$ for *S. pneumoniae* 603 growth in BHI vs. 11mM L-lactic acid. Error bars represent standard deviation. N.G. is no growth.

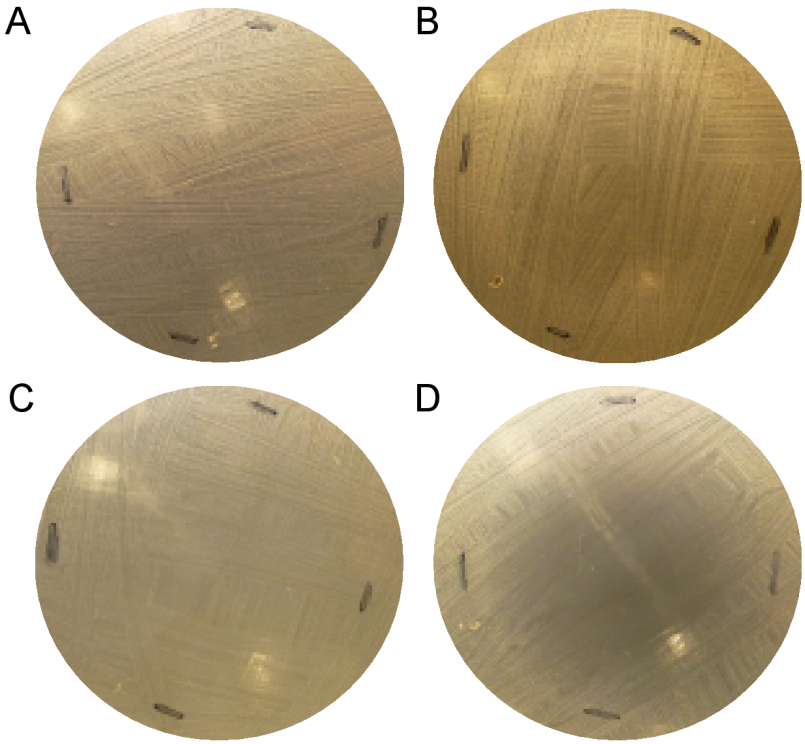

Figure 6. *D. pigrum* and *C. pseudodiphtheriticum* grown together but not *D. pigrum* alone inhibit *S. pneumoniae* in an *in vitro* agar medium-based assay. Representative images of *S. pneumoniae* 603 growth on (**A**) BHI alone or on CFCAM from (**B**) *C. pseudodiphtheriticum* KPL1989, (**C**) *D. pigrum* KPL1914 or (**D**) both *D. pigrum* and *C. pseudodiphtheriticum* grown in a mixed inoculum (n=4). To condition the medium, we cultivated *D. pigrum* and/or *C. pseudodiphtheriticum* on a membrane, which was then removed prior to spreading a lawn of *S. pneumoniae*. Images were cropped. Black marks indicate edges of where the membrane had been.

Table S1A. Adult nostril dataset ANCOM results. These Log abundance values are plotted in Figure 1A. (See excel file)

Table S1B. Pediatric nostril dataset ANCOM results. These Log abundance values are plotted in Figure 1B. (See excel file)

Table S2. *D. pigrum* is inhibited when grown directly on cell-free *C. accolens*-conditioned BHI agar supplemented with triolein. Related to Figure S2B.

	Growth of Target Strains[a]		
Conditioning Strain	*S. pneumoniae* 603 (6B)	*D. pigrum* CDC 4709-98	*D. pigrum* KPL1914
C. accolens KPL1818	0	0	0
C. propinquum[1] DSM44285	0	+	+
C. pseudodiphtheriticum KPL1989	+	+	+

[a]0, no growth; +, growth detected, $n \geq 3$

Table S3. Oleic acid inhibits *D. pigrum* growth. Related to section "Nasal *Corynebacterium* species enhance the growth of *D. pigrum in vitro*."

	ZOI (mm)[a]		
Oleic Acid (μg/disc)	*S. pneumoniae* 603 (6B)	*D. pigrum* CDC 4709-98	*D. pigrum* KPL1914
20	10.3 ± 4.7	12.0 ± 2.9	17.0 ± 2.1
50	22.0 ± 5.4	26.8 ± 4.4	28.4 ± 7.0
100	26.3 ± 6.7	35.8 ± 4.5	39.4 ± 5.0

[a]Mean ZOI ± SD produced in a disc-diffusion assay. ZOIs were measured as the smallest diameter of inhibited growth and measurements include disc diameter (6 mm). Biological replicates (*n*=4 for *S. pneumoniae*, *n*=5 for *D. pigrum*) were averaged.

Figure S1. Ten different *D. pigrum* strains inhibit methicillin-resistant *S. aureus* USA300 strain JE2. Related to Figure 3. *D. pigrum* isolates inhibited *S. aureus* strain JE2 on BHI agar (*n*≥3). Representative images are shown for each strain. *D. pigrum* was resuspended in PBS then a 5µl drop was placed onto BHI agar and pregrown for 48 hrs. After that, *S. aureus* was inoculated adjacent to the *D. pigrum*. Inhibition was assessed after 24 and 48 hrs (48 hrs shown here).

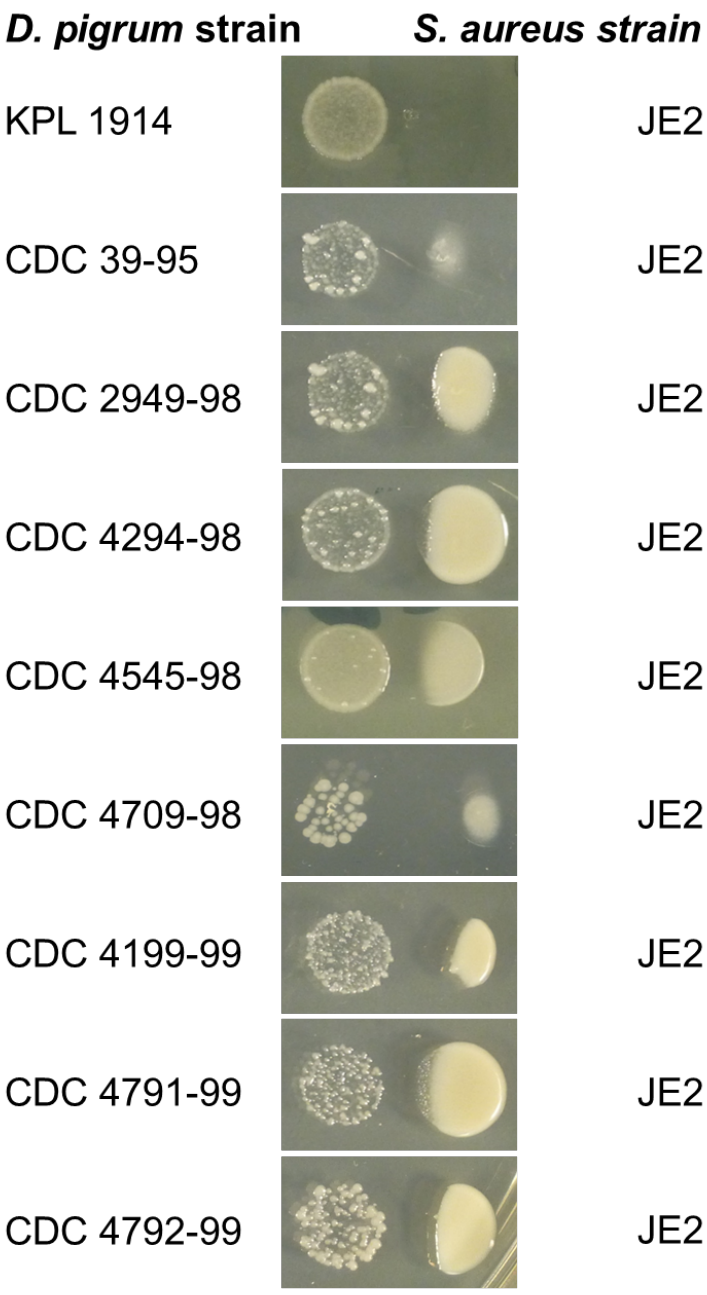

Table S4. Assembly characteristics of *D. pigrum* Illumina genomes in this study. Related to Table 1.

CDC / internal strain number		Nodes [N]	N50 [bp]	Max [bp]	Total [bp]	Reads [N]
	KPL1914	107	87,900	210,575	1,726,398	1,640,818
39-95	KPL1922	138	153,015	273,357	1,859,258	1,819,350
2949-98	KPL1930	179	127,744	456,484	1,886,398	1,699,318
4294-98	KPL1931	139	88,498	198,469	2,014,679	2,357,776
4420-98	KPL1932	134	209,743	328,871	1,934,436	2,098,746
4545-98	KPL1933	50	283,724	492,087	1,861,299	2,738,030
4709-98	KPL1934	142	110,284	268,980	1,912,682	2,198,156
4199-99	KPL1937	109	128,019	379,812	1,976,602	2,528,652
4791-99	KPL1938	129	132,767	316,186	1,873,869	1,831,854
4792-99	KPL1939	86	253,067	460,850	1,893,917	2,039,094

Figure S2. The conservative core genome of 11 *D. pigrum* strains encodes 1200 orthologs. Related to section "The genomes of 11 *D. pigrum* strains reveal a small genome and high degree of sequence conservation consistent with a highly host-adapted bacterium." A Venn diagram generated using the bidirectional best-hits (BDBH), cluster of orthologous groups (COG) triangle and OrthoMCL (OMCL) algorithms identified predicted protein orthologs (RAST annotation) shared between the 11 *D. pigrum* genomes (GET_HOMOLOGUES package version 02012019) (Contreras-Moreira and Vinuesa, 2013). Flag t=11 was used to only include clusters containing single-copy orthologs from all input species since these are likely the most reliable ortholog predictions.

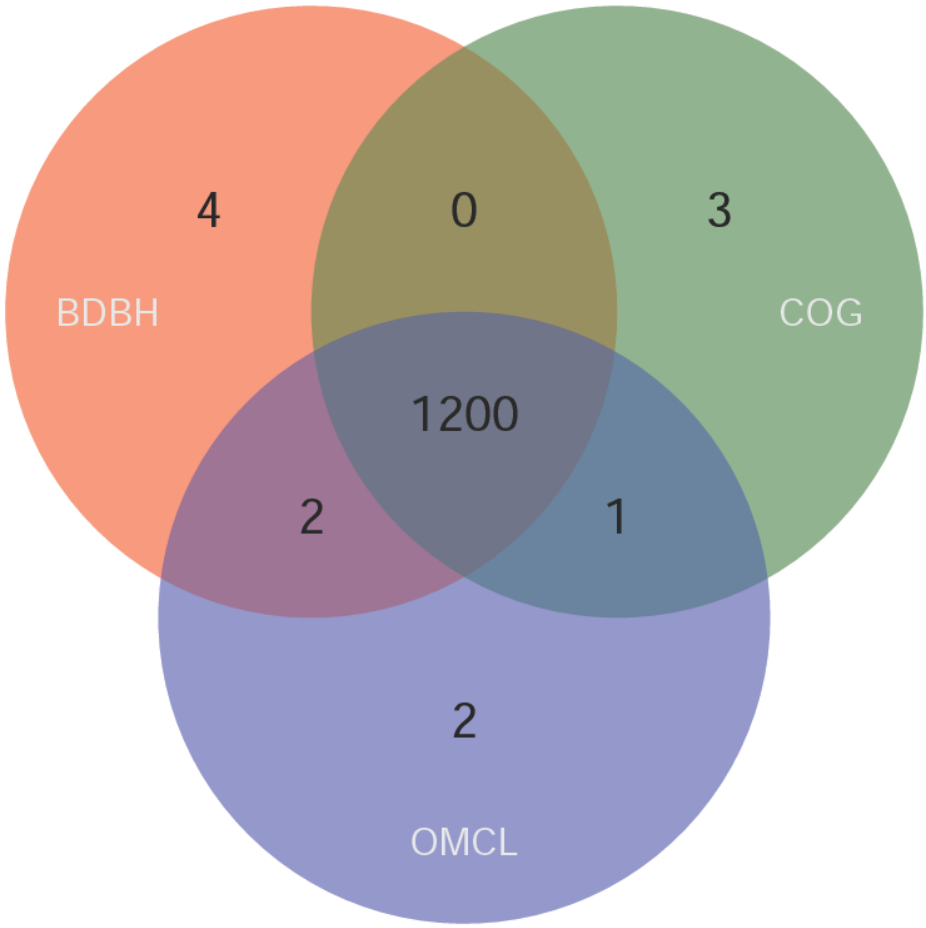

Figure S3. Core, shell and cloud pangenome of 11 *Dolosigranulum pigrum* strains. Related to section "The genomes of 11 *D. pigrum* strains reveal a small genome and high degree of sequence conservation consistent with a highly host-adapted bacterium." The pangenome of the 11 *D. pigrum* strains includes an estimated core of 1216, soft core of 116, shell of 373 and cloud of 1024 genes (CDS), as determined by the parse_pangenome_matrix.pl script (using the OMCL / COG intersection) of the GET_HOMOLOGUES package version 02012019 (Contreras-Moreira and Vinuesa, 2013). The core genome is composed of genes that are present in all strains and soft core contains clusters present in 10 genomes but not the core as defined in (Kaas et al., 2012). Cloud is defined as genes only present in a few genomes (cut-off is defined as the class next to the most populated non-core cluster class). Shell genes are the remaining genes and displayed sorted to the number of genomes in which these are present (*n*=3-9).

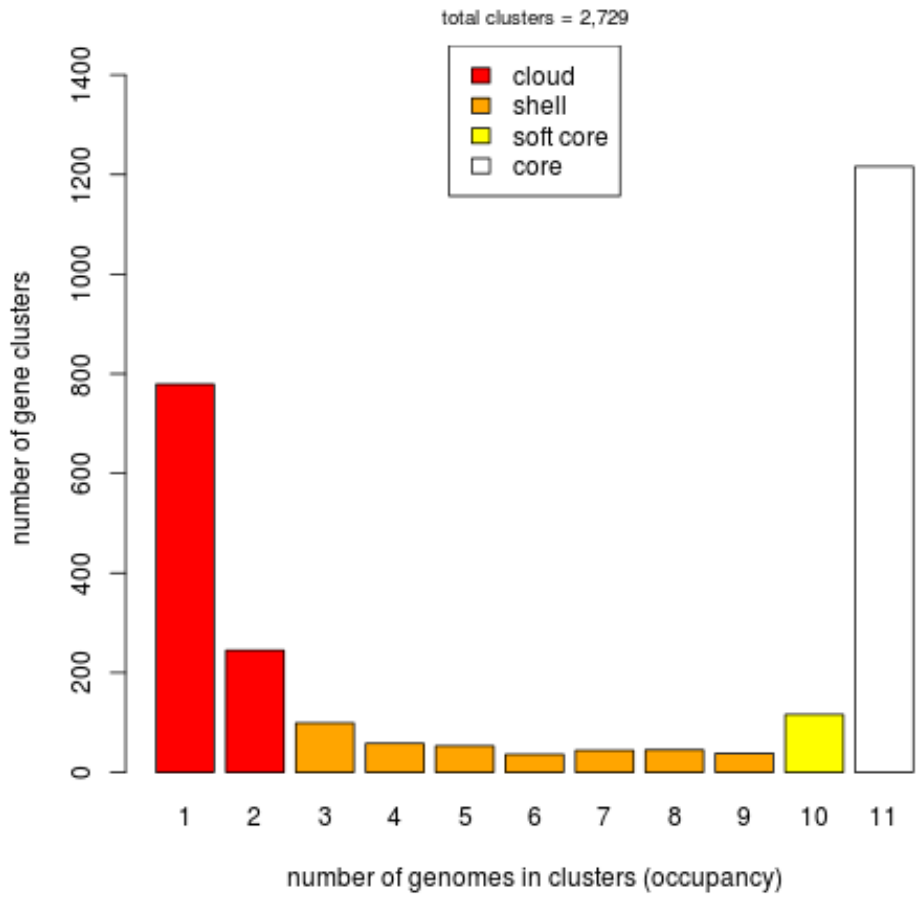

Table S5. Distribution by strain of genes in the core, soft core, shell and cloud *D. pigrum* genome.* Related to section "The genomes of 11 *D. pigrum* strains reveal a small genome and high degree of sequence conservation consistent with a highly host-adapted bacterium."

CDC or other strain #	Internal reference	Cloud [N]	Shell [N]	Soft core [N]	Core [N]
KPL1914	KPL1914	79	135	89	1216
39-95	KPL1922	81	189	109	1216
2949-98	KPL1930	88	167	113	1216
4294-98	KPL1931	243	183	110	1216
4420-98	KPL1932	134	205	114	1216
4545-98	KPL1933	102	202	96	1216
4709-98	KPL1934	105	185	111	1216
4199-99	KPL1937	186	174	94	1216
4791-99	KPL1938	73	192	108	1216
4792-99	KPL1939	110	194	108	1216
ATCC51524		68	194	108	1216

* These results were determined as described for Figure S3.

Figure S4. The (A) average nucleotide identities (ANI) and (B) amino acid identities (AAI) show a high degree of conservation across all 11 *D. pigrum* genomes. Related to section "Phylogenetic reconstruction, sequence and protein similarities." Average identity matrices of clustered coding sequences were calculated using GET_HOMOLOGUES with the OrthoMCL algorithm. Both ANI and AAI were calculated with all available clusters (t 0). Commands used: Generation of an AA identity matrix: $ ./get_homologues.pl -d "gbk-files" -A -t 0 -M and CDS identity matrix with the command $./get_homologues.pl -d "gbk files" -a 'CDS' -A -t 0 -M.

A

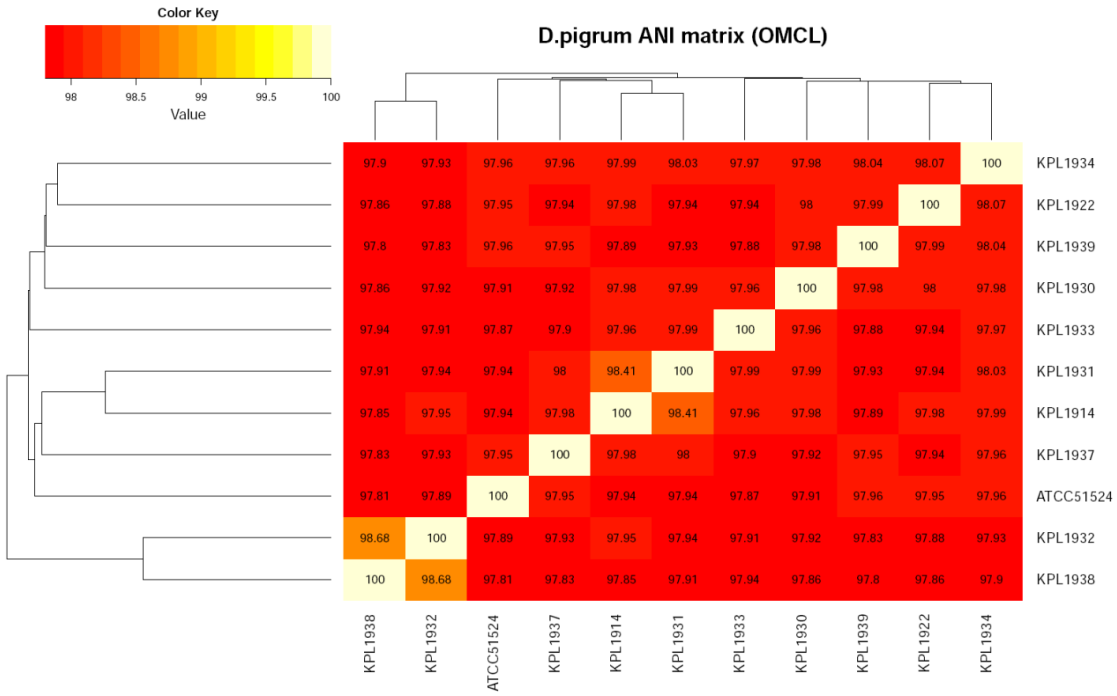

B

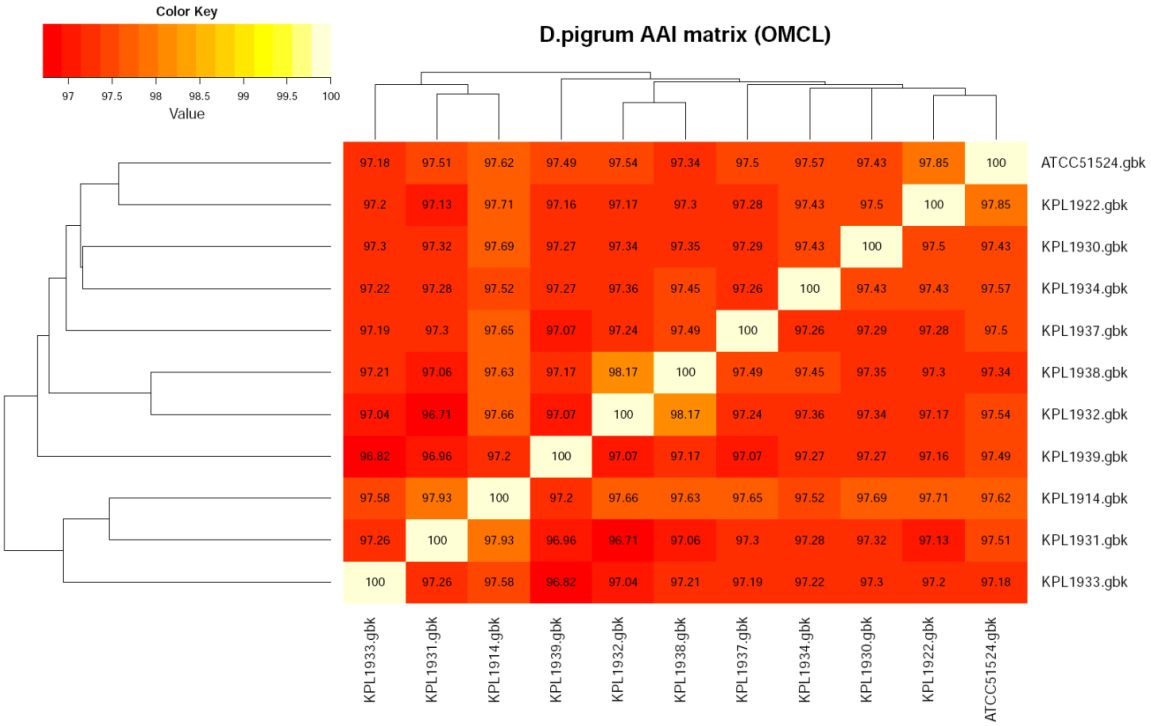

Figure S5. *D. pigrum* genomes BLAST ring comparisons. Related to Figure 4. BLAST Ring Image Generator (BRIG) version 0.95 (Alikhan et al., 2011) was used for visualization of the sequenced genomes with the closed genome of CDC 4709-98 as a reference. (**A**) Closed genome of CDC 4709-98 with GC plots (**B**) Closed genome of KPL 1914 with GC plots (**C**) BLASTN based comparison of the closed genomes of CDC 4709-98 and KPL 1914 (**D**) BLASTN based comparison of CDC 4709-98 and the remaining 10 Illumina contig-based genomes as well as ATCC 51524

5A

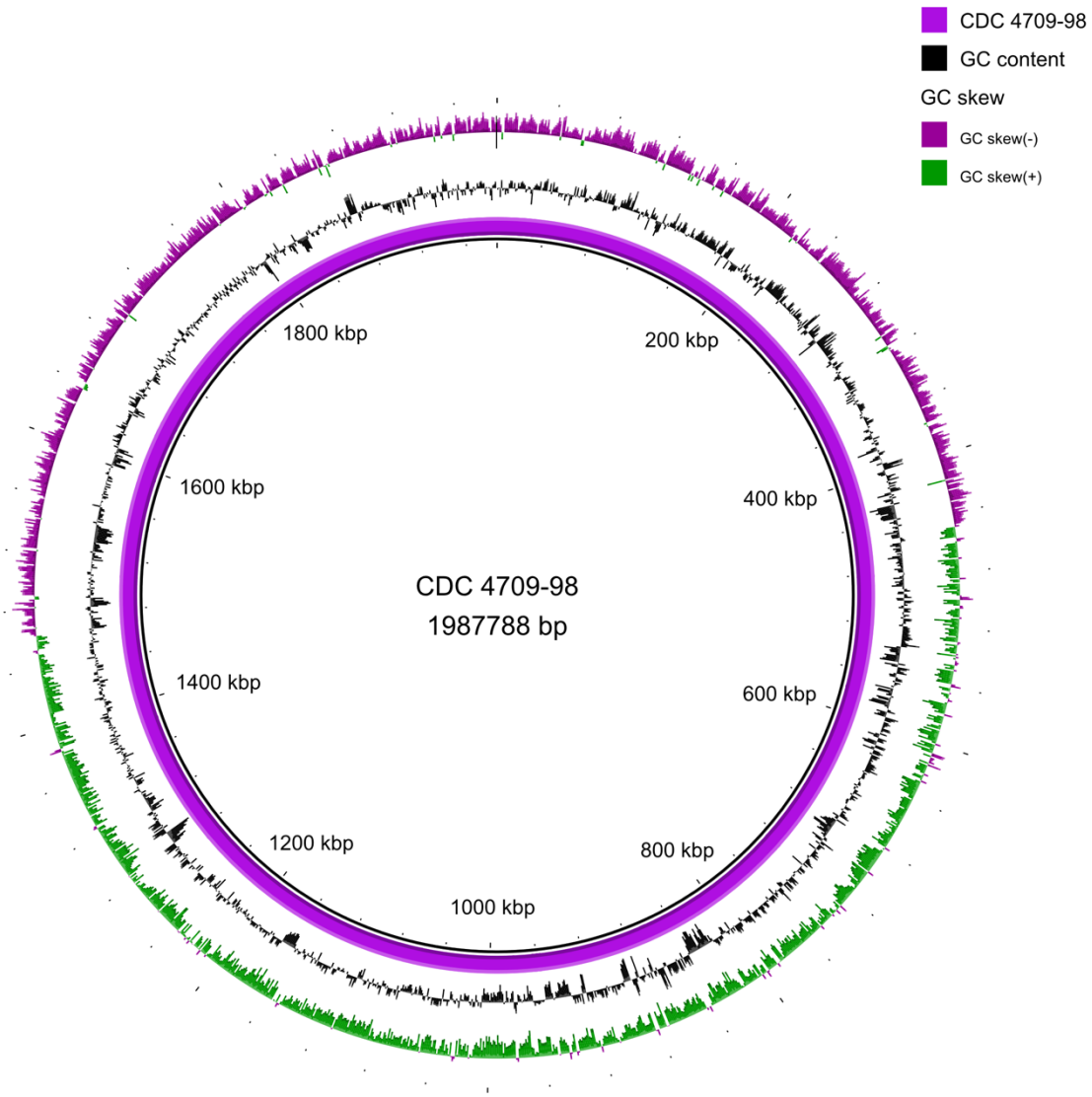

5B

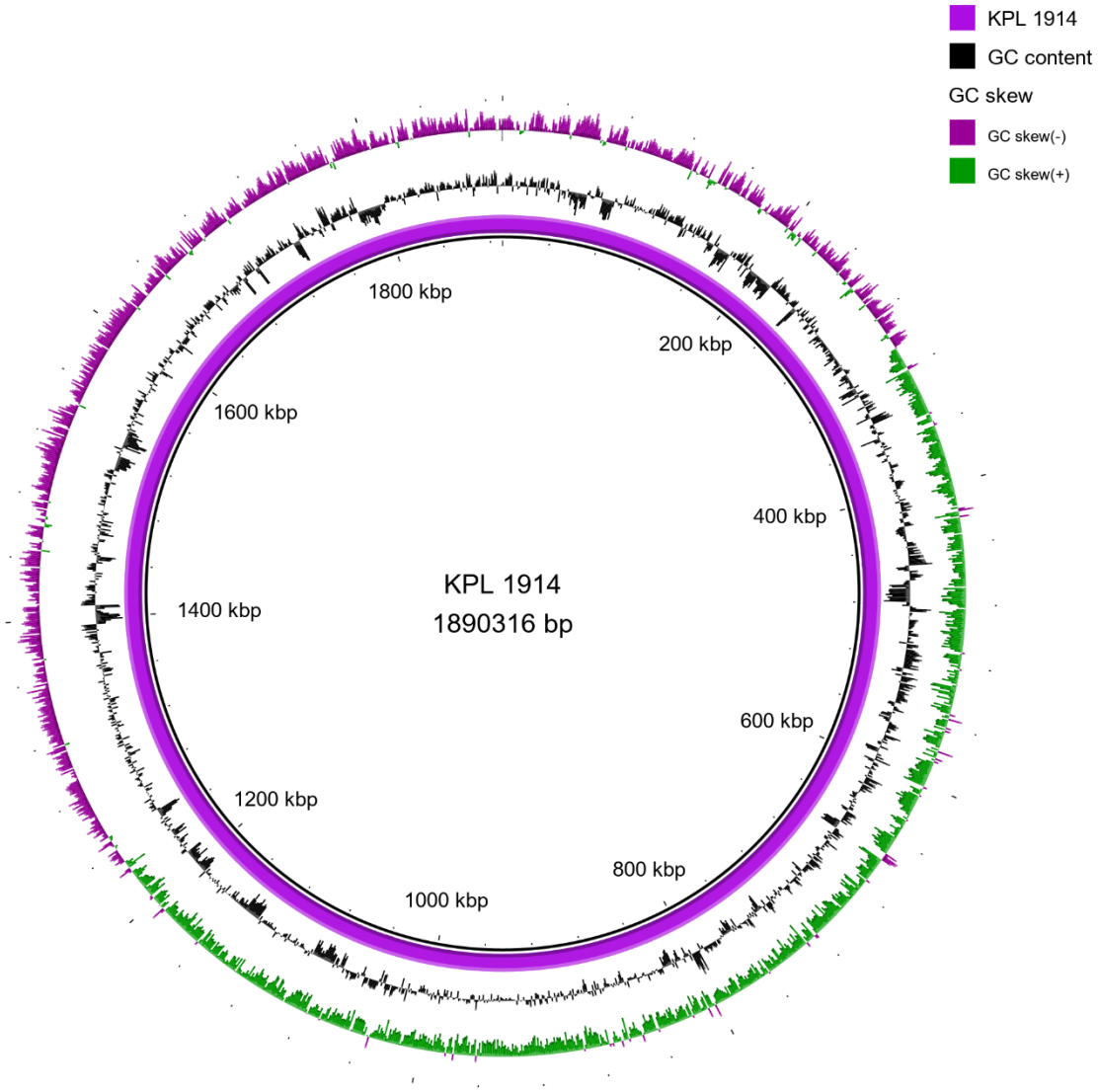

5C

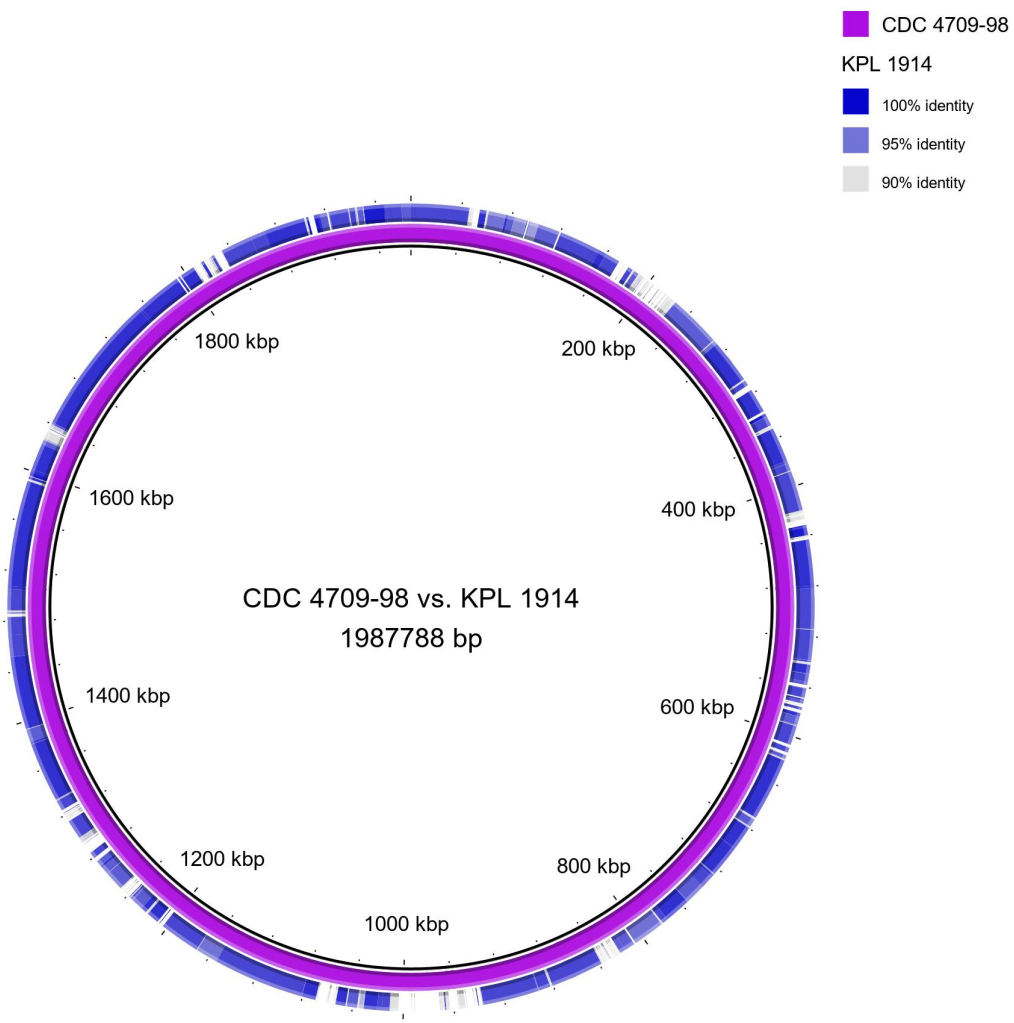

5D

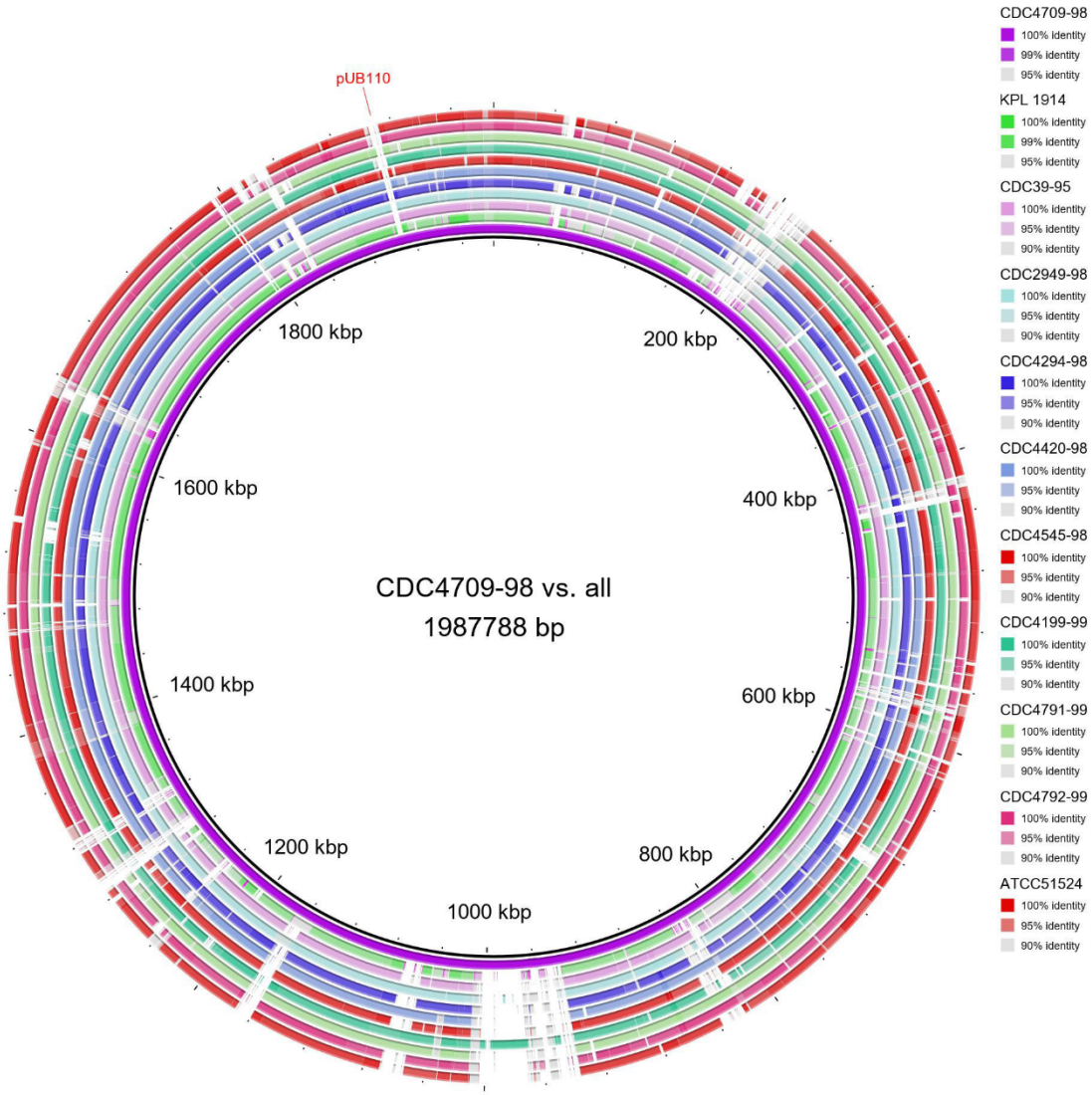

Figure S6. Phylogenetic relationship between the 11 *D. pigrum* strains. Related to section "Phylogenetic reconstruction, sequence and protein similarities." *D. pigrum* phylogenetic trees were constructed by using concatenated alignments of the intersection of predicted core genes (BDBH, COG, and OMCL, see above). Amino acids were aligned using Clustal Omega V.1.2.4 (Sievers et al., 2011) and a maximum likelihood phylogenetic tree was generated using the LG model of amino-acid replacement matrix (Le and Gascuel, 2008) as selected by smart model selection with Akaike information criterion (Lefort et al., 2017) and 100 bootstrap replicates for branch support with PhyML (phylogenetic maximal likelihood) V. 3.0 (Guindon et al., 2010) and visualized using FigTree V.1.4.4. A BIONJ distance-based tree was used as a starting tree to be redefined by the maximum likelihood algorithm. Bootstrap support values from 100 replicates are indicated above the branches. (**A**) Core genome AA tree of the 11 *D. pigrum* genomes. (**B**) Core genome AA tree with *Alloiococcus otitis* ATCC 51267 as an outgroup. Core genome size decreased to 866 clusters when including *A. otitis*.

6A

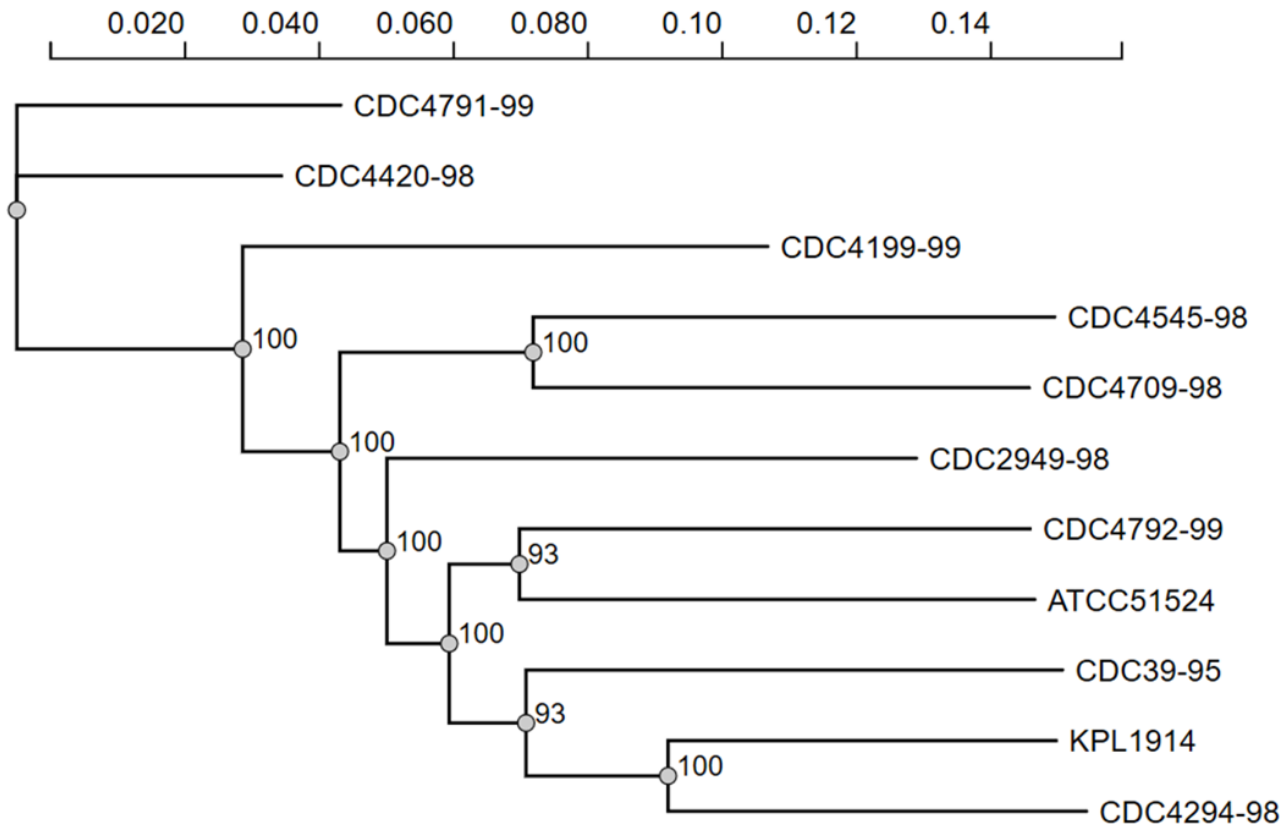

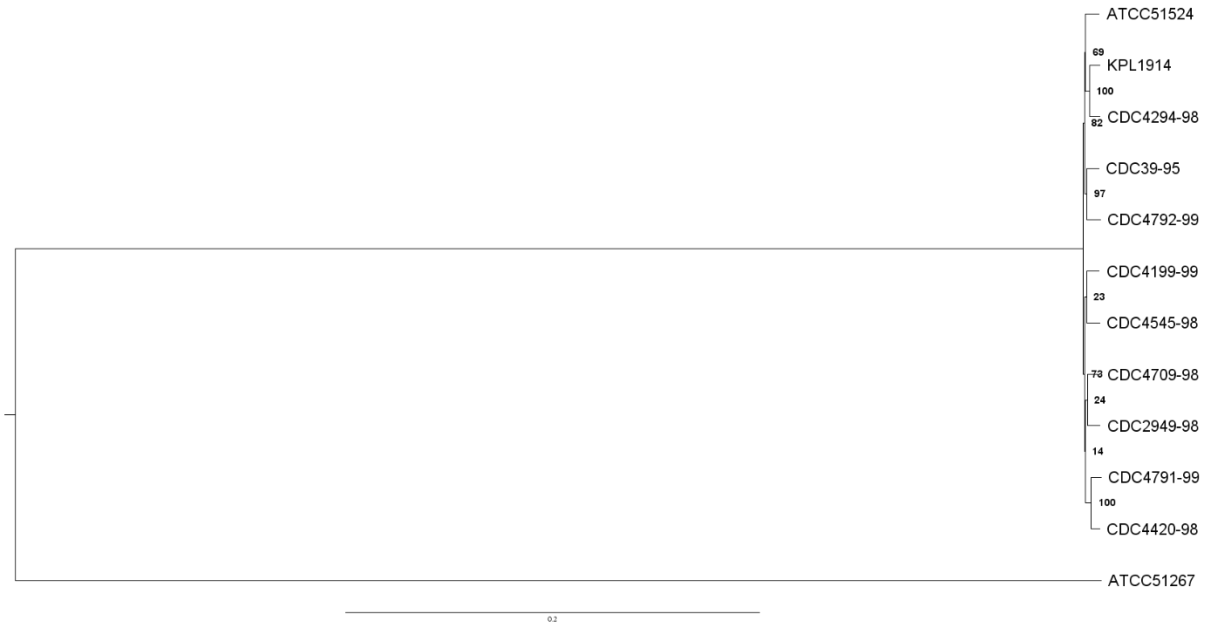

6B

Figure S7. When grown together *D. pigrum* and *C. pseudodiphtheriticum* inhibit *S. pneumoniae*. Related to Figure 6. A second set of representative images of *S. pneumoniae* 603 growth on (**A**) BHI alone or CFCAM from (**B**) *C. pseudodiphtheriticum* KPL1989, (**C**) *D. pigrum* KPL1914 or (**D**) both *D. pigrum* and *C. pseudodiphtheriticum* grown in a mixed inoculum (*n*=4). To condition the medium, we cultivated *D. pigrum* and/or *C. pseudodiphtheriticum* on a membrane, which was then removed prior to spreading a lawn of *S. pneumoniae*. Images were cropped. Black marks indicate edges of where the membrane had been.

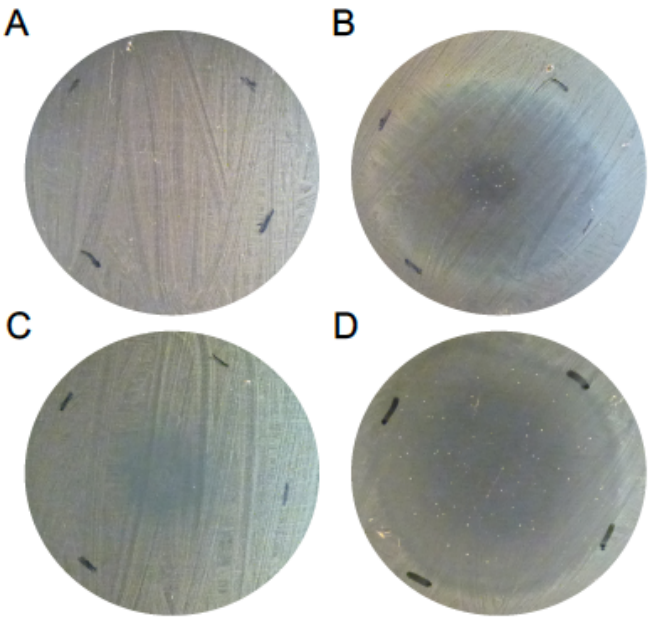

Table S6. Predicted biosynthetic gene clusters / secondary metabolites regions (antiSMASH version 5.0.0beta1-4e548fe) (Blin et al., 2019)**. Related to section "The accessory genome of 11 *D. pigrum* strains contains a diversity of biosynthetic gene clusters predicted to encode antibiotics."**

Strain	Bacteriocins	Lanthipeptides
KPL1914	2	1
39-95	1	1
2949-98	1	0
4294-98	2	0
4420-98	0	0
4545-98	1	0
4709-98	2	1
4199-99	3	0
4791-99	0	0
4792-99	2	0
ATCC51524	0	2

Table S7. Species-level reanalysis of a pediatric nostril microbiota dataset. Related to Fig.

1. (see excel file)

Figure S8. Predicted biosynthetic gene clusters / secondary metabolites regions (antiSMASH version 5.0.0beta1-4e548fe) (Blin et al., 2019)**. Related to section "The accessory genome of 11 *D. pigrum* strains contains a diversity of biosynthetic gene clusters predicted to encode antibiotics."**

KPL1914

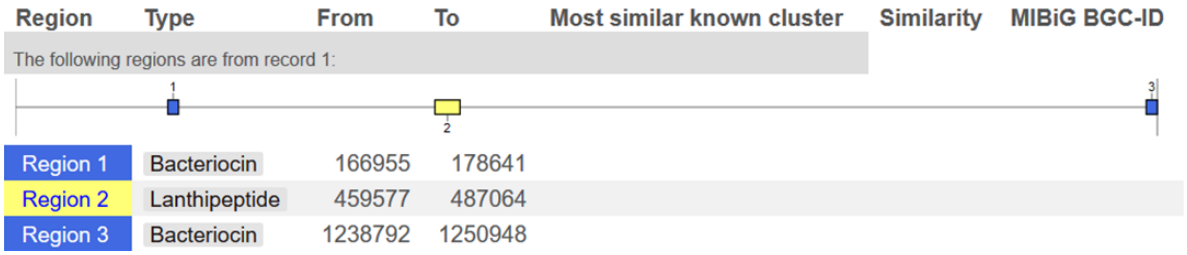

Region	Type	From	To	Most similar known cluster	Similarity	MIBiG BGC-ID
The following regions are from record 1:						
Region 1	Bacteriocin	166955	178641			
Region 2	Lanthipeptide	459577	487064			
Region 3	Bacteriocin	1238792	1250948			

CDC4709-98

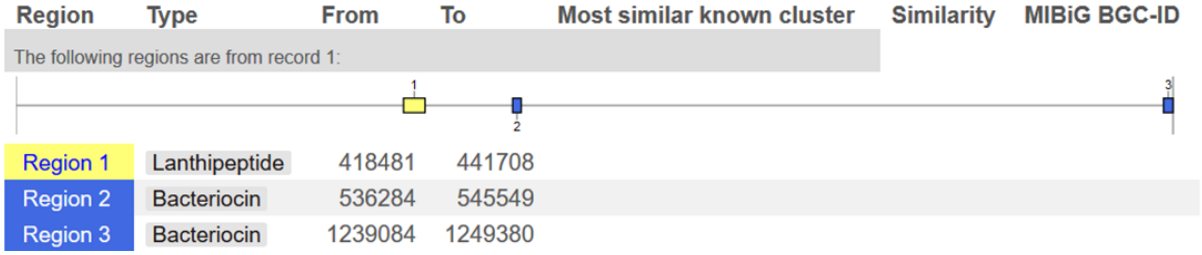

Region	Type	From	To	Most similar known cluster	Similarity	MIBiG BGC-ID
The following regions are from record 1:						
Region 1	Lanthipeptide	418481	441708			
Region 2	Bacteriocin	536284	545549			
Region 3	Bacteriocin	1239084	1249380			

CDC39-95

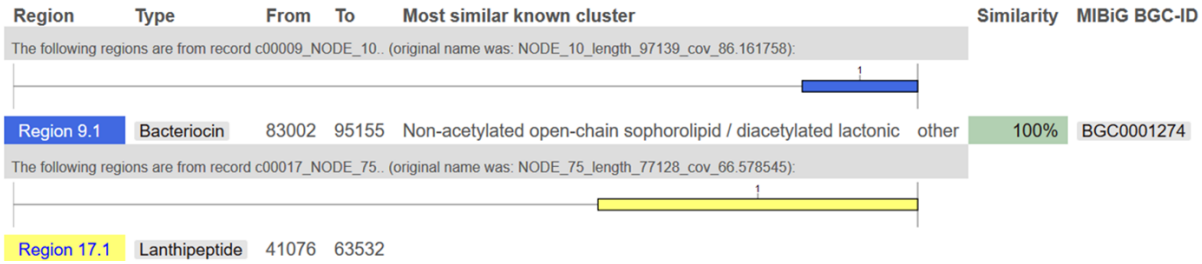

Region	Type	From	To	Most similar known cluster	Similarity	MIBiG BGC-ID
The following regions are from record c00009_NODE_10.. (original name was: NODE_10_length_97139_cov_86.161758):						
Region 9.1	Bacteriocin	83002	95155	Non-acetylated open-chain sophorolipid / diacetylated lactonic other	100%	BGC0001274
The following regions are from record c00017_NODE_75.. (original name was: NODE_75_length_77128_cov_66.578545):						
Region 17.1	Lanthipeptide	41076	63532			

CDC2949-98

Region	Type	From	To	Most similar known cluster	Similarity	MIBiG BGC-ID
The following regions are from record c00036_NODE_16.. (original name was: NODE_165_length_169774_cov_66.562698):						
Region 36.1	Bacteriocin	132959	145112			

CDC4294-98

Region	Type	From	To	Most similar known cluster	Similarity	MIBiG BGC-ID
The following regions are from record c00014_NODE_14.. (original name was: NODE_14_length_25558_cov_121.382584):						
Region 14.1	Bacteriocin	14627	25696			
The following regions are from record c00028_NODE_36.. (original name was: NODE_36_length_49203_cov_111.674515):						
Region 28.1	Bacteriocin	38167	49341			

CDC4545-98

Region	Type	From	To	Most similar known cluster	Similarity	MIBiG BGC-ID
The following regions are from record c00010_NODE_30.. (original name was: NODE_30_length_491949_cov_138.342133):						
Region 10.1	Bacteriocin	333003	345156			

CDC4199-99

Region	Type	From	To	Most similar known cluster	Similarity	MIBiG BGC-ID
The following regions are from record c00016_NODE_52.. (original name was: NODE_52_length_379674_cov_119.267921):						
Region 16.1	Bacteriocin	254448	265629			
Region 16.2	Bacteriocin	283318	295471			
The following regions are from record c00030_NODE_10.. (original name was: NODE_100_length_155311_cov_111.723755):						
Region 30.1	Bacteriocin	23742	34038			

CDC4792-99

Region	Type	From	To	Most similar known cluster	Similarity	MIBiG BGC-ID
The following regions are from record c00013_NODE_48.. (original name was: NODE_48_length_252929_cov_101.571663):						

Region 13.1	Bacteriocin	141759	153571			
Region 13.2	Bacteriocin	172804	184957			

ATCC51524

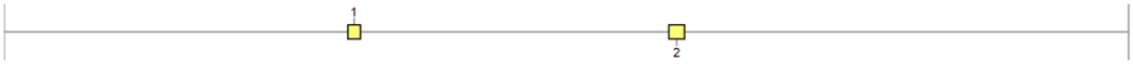

Region	Type	From	To	Most similar known cluster	Similarity
Region 1	lanthipeptide	564,388	585,116		
Region 2	lanthipeptide	1,091,260	1,117,015		

References

Alikhan, N.F., Petty, N.K., Ben Zakour, N.L., and Beatson, S.A. (2011). BLAST Ring Image Generator (BRIG): simple prokaryote genome comparisons. BMC Genomics *12*, 402.

Blin, K., Shaw, S., Steinke, K., Villebro, R., Ziemert, N., Lee, S.Y., Medema, M.H., and Weber, T. (2019). antiSMASH 5.0: updates to the secondary metabolite genome mining pipeline. Nucleic Acids Res.

Contreras-Moreira, B., and Vinuesa, P. (2013). GET_HOMOLOGUES, a versatile software package for scalable and robust microbial pangenome analysis. Appl Environ Microbiol *79*, 7696-7701.

Guindon, S., Dufayard, J.F., Lefort, V., Anisimova, M., Hordijk, W., and Gascuel, O. (2010). New algorithms and methods to estimate maximum-likelihood phylogenies: assessing the performance of PhyML 3.0. Syst Biol *59*, 307-321.

Kaas, R.S., Friis, C., Ussery, D.W., and Aarestrup, F.M. (2012). Estimating variation within the genes and inferring the phylogeny of 186 sequenced diverse Escherichia coli genomes. BMC Genomics *13*, 577.

Le, S.Q., and Gascuel, O. (2008). An improved general amino acid replacement matrix. Mol Biol Evol *25*, 1307-1320.

Lefort, V., Longueville, J.E., and Gascuel, O. (2017). SMS: Smart Model Selection in PhyML. Mol Biol Evol *34*, 2422-2424.

Sievers, F., Wilm, A., Dineen, D., Gibson, T.J., Karplus, K., Li, W., Lopez, R., McWilliam, H., Remmert, M., Soding, J.*, et al.* (2011). Fast, scalable generation of high-quality protein multiple sequence alignments using Clustal Omega. Mol Syst Biol *7*, 539.

Supplemental text

Antibiotic resistance prediction. We analyzed all 11 *D. pigrum* genomes for putative antibiotic resistance genes and mutations that confer antibiotic resistance using the Resistance Gene Identifier (RGI) on the Comprehensive Antibiotic Resistance Database (CARD) (McArthur et al., 2013) allowing only perfect and strict results. This identified a candidate in only one strain. These data are consistent with the report from LaClaire and Facklam of *D. pigrum* susceptibility to amoxicillin, cefotaxime, cefuroxime, clindamycin, levofloxacin, meropenem, penicillin, quinupristin-dalfopristin, rifampin, tetracycline, and vancomycin for all tested *D. pigrum* strains (LaClaire and Facklam, 2000). *D. pigrum* strain CDC 4709-98 alone encoded a predicted bleomycin resistance protein (BRP), which was predicted with 100% amino acid in a protein homolog model. In agreement, ResFinder (Zankari et al., 2012) identified kanamycin nucleotidyltransferase (*aadD*, aka ANT(4')-Ia, aminoglycoside adenyltransferase AAD, spectinomycin resistance; streptomycin resistance; transferase) in this strain with 99.74 % sequence identity. Detailed analysis of this region with PlasmidFinder (Carattoli et al., 2014) and BLAST (Altschul et al., 1990) revealed loci with sequence identity to portions of plasmid pUB110 from *S. aureus* (McKenzie et al., 1986) suggesting integration of, or at least part of, this plasmid into the genome of strain CDC 4709-98.

Glycolysis (Embden-Meyerhof-Parnas pathway, EMP). Enzymes present in all 11 isolates included glucokinase, glucose-6-phosphate isomerase, 6-phosphofructokinase, fructose-bisphosphate aldolase class II-1,6-bisphosphate-aldolase, triose phosphate isomerase, NAD-dependent glyceraldehyde-3-phosphate dehydrogenase, phosphoglycerate kinase, 2,3-bisphosphoglycerate-independent phosphoglycerate mutase, enolase and pyruvate kinase. Three strains (KPL1914, CDC 39-95, CDC 4792-99) also encoded a predicted fructose-bisphosphate aldolase class I (EC 4.1.2.13), whereas all strains harbored a predicted triosephosphate isomerase.

As noted in the main text, all 11 strains encoded a predicted L-lactate-dehydrogenase (EC 1.1.1.27), which catalyzes the reduction of pyruvate to lactate regenerating NAD+ for glycolysis (GAPDH step), consistent with homofermentation to L-lactate as the primary product of glycolysis. Moreover, the absence of xylulose-5-phosphate phosphoketolase (EC 4.1.2.9) is inconsistent with (obligate) heterofermentation, since bacteria that heteroferment lack aldolase and have to shunt through the pentose phosphate or phosphoketolase pathway (Buyze et al., 1957). In addition to homofermentation to lactate, some end product flexibility, which is probably produced under differing environmental/nutritional conditions, is predicted by the presence in all 11 genomes of genes needed to accomplish mixed-acid fermentation with potential production of formate, acetate and ethanol (i.e., enzymes pyruvate formate-lyase (EC 2.3.1.54), phosphate acetyltransferase (EC 2.3.1.8) and acetate kinase (EC 2.7.2.1), as well as acetaldehyde dehydrogenase (1.2.1.10) and alcohol dehydrogenase (EC 1.1.1.1)).

Identification of a V-type ATPase in all 11 isolates. V-ATPases hydrolyse ATP to drive a proton pump but cannot work in reverse to synthesize ATP.

There is no tricarboxylic acid (TCA) cycle present in *D. pigrum*. Only fumarate-hydratase (EC 4.2.1.2) and TCA associated dihydrolipoyl dehydrogenase (EC 1.8.1.4) were predicted in all *D. pigrum* genomes.

Anaerobic respiratory reductases. We did not identify butyryl-CoA-reductase (EC 1.3.8.1) or any other predicted anaerobic reductases in all *D. pigrum* strains. However, *D. pigrum* CDC 4545-98 encoded an arsenate reductase (EC 1.20.4.1).

Sialidases. The original species description of *D. pigrum* reports production of acid from D-glucose, galactose, D-fructose, D-mannose, maltose and L-fucose in two isolates with strain-level variation in producing acid from D-arabinose, mannitol, sucrose and N-acetyl-glucosamine (Aguirre et al., 1993). Glucose is the main monosaccharide detected in the nasal environment

(Krismer et al., 2014). Host-cell-surface- and host-mucin-derived sialic acids are another important potential source of monosaccharides and all 11 *D. pigrum* genomes harbor a putative sialidase as well as a predicted transporter (sodium solute symporter) and catabolic enzymes suggesting it utilizes sialic acid in the nasal passages.

Polyamine auxotrophy and transport. The absence of predicted genes required for *de novo* synthesis of the essential polyamines putrescine and spermidine indicates that *D. pigrum* likely relies on extracellular polyamines. Consistent with this, all strains harbor putative ABC type spermidine transporter components (SPERta, SPERtb, SPERtc, SPERtd) adjacent to each other as well as putative putrescine transporter genes (*potA*, *potB*, *potC*, and *potD*).

Nicotinic acid (niacin) auxotrophy and transport. NAD and NADP are critical factors for cellular metabolism**.** However, *D. pigrum* lacked known genes for *de novo* synthesis and for salvage of nicotinate or nicotinamide. However, the presence of *niaP* predicts uptake of nicotinic acid (niacin) by all 11 strains. All strains also encoded genes needed to convert niacin or nicotinamide to NAD+ and NADP: nicotinamidase (EC 3.5.1.19), nicotinate phosphoribosyltransferase (EC 2.4.2.11), nicotinate-nucleotide adenylyltransferase (EC 2.7.7.18), NAD synthetase (EC 6.3.1.5), NAD kinase (EC 2.7.1.23) and NadR transcriptional regulator.

Biotin auxotrophy and transport. A biotin uptake system was predicted in all 11 *D. pigrum* strains (Substrate-specific component BioY of biotin ECF transporter) and no biosynthesis was predicted. Biotin-protein ligase (EC 6.3.4.15) was predicted only in KPL1914 and ATCC51524.

Methionine auxotrophy and degradation. All 11 *D. pigrum* genomes lacked a complete known pathway for methionine biosynthesis. Methionine has been reported to be a limiting nutrient in the nasal passages of humans and its synthesis is upregulated in *S. aureus* growing in synthetic nasal medium (Krismer et al., 2014). In contrast, all 11 encoded two full sets of the genes required for

methionine degradation in different regions on their chromosome suggesting external dependence. Each set includes *metN* (methionine ABC transporter ATP-binding protein), *metP* (methionine ABC transporter permease protein), *metQ* (methionine ABC transporter substrate-binding protein) and *metT* (methionine transporter).

Glutamine. Glutamine synthetase I (EC 6.3.1.2) was predicted in all 11 strains and catalyzes the reaction of L-glutamine from L-glutamate and NH_4^+ using ATP. Glutamate racemase (EC 5.1.1.3) was predicted in all 11 and catalyzes D- / L-glutamate interconversion. NAD(P)-specific glutamate dehydrogenase (EC 1.1.1.4) GdhA was predicted in all 11 and catalyzes the formation of L-glutamate and H_2O from 2-oxoglutarate, ammonia and $NADH+H^+$ and vice versa.

References

Aguirre, M., Morrison, D., Cookson, B.D., Gay, F.W., and Collins, M.D. (1993). Phenotypic and phylogenetic characterization of some Gemella-like organisms from human infections: description of Dolosigranulum pigrum gen. nov., sp. nov. J Appl Bacteriol *75*, 608-612.

Altschul, S.F., Gish, W., Miller, W., Myers, E.W., and Lipman, D.J. (1990). Basic local alignment search tool. J Mol Biol *215*, 403-410.

Buyze, G., Van Den Hamer, C.J., and De Haan, P.G. (1957). Correlation between hexosemonophosphate shunt, glycolytic system and fermentation-type in Lactobacilli. Antonie Van Leeuwenhoek *23*, 345-350.

Carattoli, A., Zankari, E., Garcia-Fernandez, A., Voldby Larsen, M., Lund, O., Villa, L., Moller Aarestrup, F., and Hasman, H. (2014). In silico detection and typing of plasmids using PlasmidFinder and plasmid multilocus sequence typing. Antimicrob Agents Chemother *58*, 3895-3903.

Krismer, B., Liebeke, M., Janek, D., Nega, M., Rautenberg, M., Hornig, G., Unger, C., Weidenmaier, C., Lalk, M., and Peschel, A. (2014). Nutrient limitation governs Staphylococcus aureus metabolism and niche adaptation in the human nose. PLoS Pathog *10*, e1003862.

LaClaire, L., and Facklam, R. (2000). Antimicrobial susceptibility and clinical sources of Dolosigranulum pigrum cultures. Antimicrob Agents Chemother *44*, 2001-2003.

McArthur, A.G., Waglechner, N., Nizam, F., Yan, A., Azad, M.A., Baylay, A.J., Bhullar, K., Canova, M.J., De Pascale, G., Ejim, L., *et al.* (2013). The comprehensive antibiotic resistance database. Antimicrob Agents Chemother *57*, 3348-3357.

McKenzie, T., Hoshino, T., Tanaka, T., and Sueoka, N. (1986). The nucleotide sequence of pUB110: some salient features in relation to replication and its regulation. Plasmid *15*, 93-103.

Zankari, E., Hasman, H., Cosentino, S., Vestergaard, M., Rasmussen, S., Lund, O., Aarestrup, F.M., and Larsen, M.V. (2012). Identification of acquired antimicrobial resistance genes. The Journal of antimicrobial chemotherapy *67*, 2640-2644.